Topaz magmatic crystallization in rhyolites of the Central Andes (Chivinar volcanic complex, NW Argentina): constraints from texture, mineralogy and rock chemistry

Gioncada Anna[a], Orlandi Paolo[a], Vezzoli Luigina[b], Omarini Ricardo H.[c], Mazzuoli Roberto[a], Lopez-Azarevich Vanina[c], Sureda Ricardo[c], Azarevich Miguel[c], Acocella Valerio[d], Ruch Joel[d]

[a] *Dipartimento di Scienze della Terra, Università degli Studi di Pisa, Pisa, Italy*

[b] *Dipartimento di Scienza e Alta Tecnologia, Università dell'Insubria, Como, Italy*

[c] *Facultad de Ciencias Naturales, Universidad Nacional de Salta, CEGA-CONICET Salta, Argentina*

[d] *Dipartimento di Scienze, Università Roma Tre, Roma, Italy*

Corresponding author: A.Gioncada gioncada@dst.unipi.it

Abstract: Topaz-bearing rhyolite lavas were erupted as domes and cryptodomes during the early history of the Late Miocene Chivinar volcano, in Central Andes. These are the only topaz rhyolite lavas recognized in Central Andes. Textural, mineralogical and geochemical data on the Chivinar rhyolites suggest that topaz crystallized from strongly residual, fluorine-rich, peraluminous silicate melts of topazite composition before the complete solidification of the lava domes. Crystallization of the rhyolitic magma began with sodic plagioclase and alkali feldspar phenocrysts in the magma chamber, followed by groundmass quartz+alkali feldspar+minor sodic plagioclase during dome emplacement, and terminated with quartz+topaz+vapour bubbles forming small scattered miaroles. Fluorine partitioning into the fluid phase occurred only in the final stage of groundmass crystallization. The magmatic origin of topaz indicates the presence of a fluorine-rich highly differentiated magma in the early history of the Chivinar volcano and suggests the possibility of rare metals mineralizations related to the cooling and solidification of a silicic magma chamber. A late fluid circulation phase, pre-dating the andesitic phase of the Chivinar volcano, affected part of the topaz rhyolite lavas. The presence of Nb, Ta and Mn minerals as primary accessories in the rhyolites and as secondary minerals in veins suggests a connection of the fluid circulation phase with the silicic magmatic system. Although at the edge of the active volcanic arc, the Chivinar topaz rhyolites are in correspondence of the transtensive Calama-Olacapato-El Toro fault system, suggesting preferred extensional conditions for the formation of magmatic topaz in convergent settings, consistently with evidence from other known cases worldwide.

Key words: Topaz-bearing rhyolite, fluorine, magmatic volatiles, miarolitic texture, Central Andes

47 1. Introduction

48

49 Although more frequently interpreted as the product of post-magmatic vapour-phase alteration (e.g.;
50 Taylor, 2009), topaz is also a rare primary constituent of magmatic rocks, originated by the
51 crystallization of peraluminous and fluorine-rich silicic magmas (Scaillet and MacDonald, 2004;
52 Lukkari, 2002; Agangi et al., 2010). The silicatic melts enriched in fluorine have particular physical
53 properties, i.e. low viscosity and density (Aiuppa et al., 2009). These enhance the efficiency of the
54 petrogenetic processes, allowing segregation of unusually low fractions of partial melt from the
55 source, as well as favouring crystal-melt fractionation during magma ascent. By that, fluorine (F)
56 promotes the production and release of very small volumes of felsic magma enriched in a wide
57 variety of incompatible elements (Keppler, 1993) and, consequently, potentially related to
58 economically interesting ore mineralizations (e.g.; Burt et al., 1982; Xie et al., 2013).
59 In this paper we report the occurrence and the mineralogical, petrographic and chemical
60 characteristics of rhyolitic lavas bearing topaz from the Late Miocene Chivinar volcano, located in
61 Central Andes (Fig. 1; Koukharsky et al., 1991; Orlandi et al., 2011). While several high-silica,
62 topaz-bearing rhyolitic lavas of Cenozoic age have been recognized in North America (western
63 United States and Mexico; Christiansen et al., 1986; Huspeni et al., 1984; Sinclair, 1986;
64 Rodríguez-Ríos et al., 2007), the Chivinar topaz rhyolites are, to date, the only occurrence in the
65 Andes of South America.
66 Owing to their location at the intersection of the Andean active magmatic arc with a major NW-
67 striking fault system (Fig. 1A) and to their peculiar mineralogy, the Chivinar rocks present a two-
68 fold interest. First, the knowledge of the petrogenetic processes responsible for the composition of
69 these lavas may add new elements for the interpretation of the genesis and evolution of magmas at
70 the arc-back-arc boundary in Central Andes (Matteini et al., 2002; Acocella et al., 2011). Second,
71 understanding the origin of topaz in magmatic rocks may contribute to explain mineralizations in
72 rare, economically interesting elements (Xie et al., 2013 and references therein). For both purposes,

the determination of the primary (magmatic) vs. secondary (hydrothermal) origin of topaz is crucial. This contribution presents the textural, mineralogical and geochemical constraints to the magmatic origin of topaz in the Chivinar rhyolite and proposes a model for the magmatic crystallization of topaz rhyolite.

2. Geological framework

Cerro Chivinar is a Miocene volcano located in the western Puna plateau of the Central Andes (24º14'S – 67º27'W; 5125 m above sea level, a.s.l.), at the intersection between the N-S trending active magmatic arc (Western Cordillera) and the NW-SE trending Calama-Olacapato-El Toro (COT) transtensive fault zone (Salfity, 1985; Acocella et al., 2011) (Figs. 1A and 1B). The COT fault zone coincides with a well-defined volcanic belt, consisting of stratovolcanoes, lava domes and some monogenetic scoria centres and formed in the last 15 Ma. The composition of the magmas erupted along the COT volcanic belt includes calcalkaline magmas ranging from basaltic andesites to dacites and rhyolites, and shoshonitic magmas erupted at the mafic monogenetic scoria centres (Acocella et al., 2011 and references therein).

The geology of the Chivinar volcano has been never described in detail. The main geological features were formerly sketched in Koukharsky and Munizaga (1990) and Koukharsky et al. (1991), reporting the occurrence of topaz in the rhyolitic lavas of the volcano. Our new geologic field mapping shows that Chivinar is a polygenetic volcanic complex built by three superposed and distinct eruptive packages (Figs. 1C and 2A). The oldest unit is made up of a cluster of topaz rhyolite lava domes exposed on the N and W basal platform of the volcano, between 3500 and 4000 m a.s.l.. The following unit consists of radially emplaced coarse dacite breccia and pumice deposits that resulted from lava dome catastrophic destruction events. Finally, an andesite lava cone caps the volcanic edifice. A K/Ar age of 9.0±0.4 Ma was determined on andesite of the Chivinar lava cone

(Koukharsky and Munizaga, 1990). The substratum of the volcano is represented by continental terrigenous and evaporitic deposits of Late Eocene-Miocene age (Fig. 1B; Geste, Pozuelos and Sijes Formations; Jordan and Alonso, 1987; Blasco et al., 1996). The most active tectonic systems are WNW-ESE trending transtensive and extensional faults (Figs. 1 and 2), similarly to the ones found along the eastern continuation of the COT (Acocella et al., 2011). These systems seem also to control the preferred WNW-ESE elongation of the volcano.

The Chivinar topaz rhyolites consist of a group of coalescent lava domes that were extruded as small, endogenous lava domes and shallowly emplaced intrusive domes and plugs (Fig. 1C). The lava emplacement lacks of associated explosive products. Field evidence excludes the association of the rhyolite with one or more caldera structures. Rhyolite rests directly on or intrudes the Eocene-Miocene sedimentary substratum (Fig. 2B). Intrusive and cooling histories of individual lava bodies are locally constrained by lava textures, as marginal vitrophyres, flow-banding and breccias, at the contact with host sediments. The remnant domes range from 0.3 to 1 km in diameter and are up to 250 m high. The rhyolite dome field makes up nearly one third of the volume of the Chivinar complex.

At the end of the oldest Chivinar eruptive episode, the rhyolite lavas were intensely deformed, eroded and altered. The pervasiveness of the deformation and hydrothermal alteration contrasts with the fresh younger breccias and lavas that make up the rest of the edifice, suggesting that tectonism and fluid circulation followed by exogenous weathering occurred prior to renewed construction of the edifice.

3. Sampling and analytical methods

Three samples of the rhyolitic domes showing no macroscopic evidence of alteration were selected for the preparation of polished thin sections and for crushing and powdering. TG-9 rhyolite

125 represents the external part of a dome near the contact with the host evaporitic rock; TG-10 and TG-
126 16 come from the inner part of the coalescent dome cluster (Figs. 1C and 2). Also, three samples of
127 the rhyolites were collected from outcrops showing hydrothermal alteration evidence, to evaluate
128 the relationships between the primary and secondary mineralogy. Finally, representative samples of
129 the Chivinar dacites and andesites capping the volcanic edifice were selected for comparing the
130 major elements composition with the silicic lavas.
131 Whole-rock X-ray fluorescence (XRF) analyses of major oxides were done on fused samples with
132 an ARL 9400 XPp instrument at the Dipartimento di Scienze della Terra, University of Pisa, Italy.
133 Accuracy is 4–7% for concentrations <1 wt%, 2–4% for concentrations 1–10 wt%, 1% for
134 concentrations >10 wt%. Trace-element analyses and Loss on Ignition determinations were carried
135 out on powdered rock samples at Acme Laboratories, Ontario, Canada.
136 Microanalytical data were collected on polished and carbon-coated rock sections with a Philips
137 XL30 scanning electron microscope equipped with microanalysis EDAX (standard-less software
138 DXi4) at Dipartimento di Scienze della Terra, University of Pisa, Italy (acceleration voltage 20 kV,
139 beam current 5 nA, live time 100 s). The accuracy is better than 0.5% if abundance is >15 wt%, 1%
140 if abundance is around 5 wt%, and better than 20% if abundance is around 0.5 wt%.
141 Mineral separations were carried out to investigate the heavy mineral fraction by means of SEM-
142 EDS with the above described facilities. XRD analysis of selected mineral grains were carried out at
143 Dipartimento di Scienze della Terra, University of Pisa with a Gandolfi camera (114.6 mm in
144 diameter) and CuKα radiation.
145
146
147 4. Petrography and mineral chemistry
148
149 The Chivinar rhyolites are characterized by a very homogeneous white to creamy white colour. The
150 hand samples show porphyritic texture, with about 10 % in volume of transparent phenocrysts, 0.5

151 to 3 mm in size, rare coloured minerals, <1 mm in size, and very fine voids. No xenocrysts nor
152 xenoliths from the andesitic magmatic system have been found in the silicic lava samples.
153 The phenocrysts are plagioclase, consisting of euhedral stubby oligoclase with moderate direct
154 zoning, and sanidine, with low 2V angle (15-20°), with elongated lath shape and lower size than
155 plagioclase (Figs. 3 and 4A-B; Table 1). In sample TG-9, oligoclase is the only phenocryst.
156 The groundmass of the Chivinar rhyolites is holocrystalline and shows a fine-grained (40-100
157 microns), isotropic granular texture, consisting of equant subidiomorphic quartz, alkali feldspar and
158 sodic plagioclase (Fig. 4B-C). The quartz microlites locally show rounded corners.
159 Trails of minute vapour-rich secondary fluid inclusions cross-cutting phenocrysts are rather
160 common (Fig. 4A). The groundmass crystals mainly host solid inclusions of accessory minerals and
161 minute vapour-rich inclusions of primary formation.
162 Voids, mainly 50-200 microns in size, are disseminated in the lavas. The void boundaries are
163 irregular, following the boundaries of the rock crystals, which sometimes protrude into the void.
164 The composition of plagioclase phenocrysts is quite constant, with modest direct zoning $An_{15}Ab_{79}$-
165 $An_{10}Ab_{85}$, and the groundmass microlites have the same composition of the phenocryst's rims. The
166 composition of alkali feldspar covers the range $Or_{65}Ab_{35}$-$Or_{51}Ab_{47}$ from phenocrysts to groundmass
167 microlites (Fig. 3). The alkali feldspar crystals in the groundmass show subtle lamellae of Na-rich
168 feldspar, 0.5-1 microns thick (Fig. 4D), developing preferentially from the rim inward.
169 The average volume proportions of quartz, plagioclase and alkali feldspar in the rocks are 36±2,
170 14±3 and 49±2 vol. %, respectively, determined with image analysis using microphotos and
171 backscattered electrons SEM images (ImageJ version 1.42q). Several other minerals occur in <3
172 vol. % to trace amounts, including topaz, magnetite, both interstitial and included in quartz,
173 ilmenite, a F-bearing tri-octahedral mica (montdorite/fluor-phlogopite; see Table 1), calcic
174 amphibole, zircon and xenotime-Y. Zircon and xenotime-Y are commonly included in feldspar
175 phenocrysts (Fig. 4B). In addition, topaz, zircon and xenotime sometimes show crystallization with
176 idiomorphic terminations in voids (Fig. 4E-F).

177 Other accessories have been identified in the heavy mineral fraction (see below). In sample TG-9,
178 muscovite-like di-octahedral mica minerals are disseminated as clusters of fine-grained flakes in the
179 groundmass of the lava (Table 1; Fig. 4H).
180 Topaz is easily encountered in the samples TG-10 and TG-16, while it is sporadic in TG-9; it occurs
181 in the matrix in association with quartz, or forms glomeroporphyric aggregates of acicular crystals
182 as described in Arizona ongonites (Kortemeier and Burt, 1988). In samples TG-10 and TG-16 it
183 concentrates in particular in correspondence of clusters of voids (e.g.; Fig. 4C-G), with both
184 allotriomorphic and idiomorphic crystals.
185 The heavy mineral concentrates of the Chivinar topaz-bearing samples reveal a variety of accessory
186 minerals in the fraction with density higher than 2.9 g/cm^3, which represent between 1 and 2 wt% in
187 the studied samples. The most abundant mineral phase is topaz, representing around 50% by weight
188 of the heavy fraction (Fig. 4F), followed by a Nb-rich rutile variety. Monazite-(Ce), xenotime-(Y,
189 REE), an Fe-bearing tourmaline variety, zircon (with Th, U and Hf) and Mn-garnet (spessartine) are
190 present in trace amounts. All these mineralogical phases have been identified by SEM-EDS semi-
191 quantitative chemical analyses (Table 1). The content of Nb in the presumed rutile resulted
192 remarkably high; therefore, the identification was confirmed by an X-ray powder pattern collected
193 with a Gandolfi camera.
194 In the samples from the outcrops affected by hydrothermal alteration, the rhyolitic lavas show the
195 same primary mineralogy and texture of the unaltered samples. They are porphyritic, with
196 millimetric plagioclase and sanidine phenocrysts in a quartz-feldspathic groundmass. The secondary
197 minerals are both disseminated and in veinlets that stand out for their dark green to black colour
198 (Fig. 4I-J) and include Mn-bearing silicates (Mn-bearing sodic amphibole and sodic pyroxene), Mn-
199 bearing Fe-Ti oxides of the magnetite and ilmenite series, Mn-bearing apatite and Nb-Ta-bearing
200 rutile (Table 2). Secondary alkali feldspar occurs in the host rock at the vein contact (Table 2). In
201 some places, instead, alteration resulted in complete leaching of feldspars and silicification, with the

202 resultant rock composed of relict fine-grained quartz and scattered Nb-Ta-bearing rutile and
203 secondary silica phases.
204 The rocks of the Chivinar volcanic units following the rhyolitic lava domes are mainly andesitic
205 lavas and minor pumiceous deposits. They are porphyritic, with phenocrysts of plagioclase and
206 hornblende, minor orthopyroxene and scarce clinopyroxene, biotite and Fe-oxides in a groundmass
207 made of the same mineral phases and a variable amount of glass. The least evolved andesite
208 samples show abundant olivine phenocrysts with iddingsite rims.
209
210
211 5. Whole-rock major and trace element composition
212
213 The composition of the Chivinar topaz-bearing lavas falls in the TAS diagram in the rhyolite field,
214 with a Na_2O+K_2O around 8 wt% (Fig. 5A) and $K_2O/Na_2O = 1$ (Table 3). The rhyolites with silica
215 around 75-77 wt% are peraluminous and corundum appears in their CIPW norm, while the TG-9
216 rhyolite with 74 wt% SiO_2 is metaluminous. The composition of other volcanic rocks forming the
217 Chivinar volcanic complex is remarkably different, ranging in silica from 59 to 63 wt% (Fig. 5A):
218 the pumice clasts in the pyroclastic breccias are dacites and the final lava flows are andesites,
219 belonging to the high-K calcalkaline series.
220 A comparison of the Chivinar rhyolites with other topaz-bearing silicic rocks indicates similarly
221 high Rb, Th, U, Pb, and Y but even higher Nb, Ta, while the LREE values are lower (e.g.;
222 Christiansen et al., 1983; 1986; 2007; Lukkari, 2002; Rodríguez-Ríos et al., 2007) (Fig. 5B, C). The
223 REE patterns are notably flat, with $(La/Yb)_n = 2.5$, and display a strong Eu negative anomaly, with
224 $Eu/Eu^* = 0.11$ (Fig. 5B).
225 The Chivinar rhyolites have the same geochemical characteristics (P_2O_5 <0.1 wt%, Al_2O_3 <14.5
226 wt%, SiO_2 >73 wt%) of the low-P_2O_5 subtype of topaz-granites after Taylor and Fallick (1997), and
227 of low-P_2O_5 granites from Central Europe and Scandinavian described by Breiter (2012) and

228 Lukkari (2002). The low P_2O_5 in the Chivinar topaz rhyolites is in agreement with the absence of
229 apatite as accessory (all Ca contributed to plagioclase) and contributes to distinguish these silicic
230 magmas from S-type peraluminous magmas, suggesting a derivation by partial melting of an
231 igneous protolith rather than of a pelitic one. In the discrimination diagram suggested by Whalen et
232 al. (1987) for granites, the Chivinar topaz rhyolites fall in the field for intraplate settings (Fig. 6).
233 The North America topaz rhyolites show the same major elements characteristics and similarly high
234 Nb content and Nb/Y value (Fig. 6), and are explained with melting of continental crust previously
235 intruded by mafic magmas with an intraplate signature (Christiansen et al., 2007; Rodríguez-Ríos et
236 al., 2007).
237
238
239 6. Discussion
240
241 Whether topaz has a late magmatic (primary) or hydrothermal (secondary) origin has been a matter
242 of discussion for several silicic igneous complexes. There is abundant petrographic evidence for
243 topaz having formed as a liquidus phase in many topaz granites (Taylor, 1992, Lukkari, 2002) and,
244 also, in sub-volcanic rhyolites (Xie et al., 2013). Indeed, the occurrence of melt inclusions in topaz
245 has been taken as a proof of a magmatic origin for topaz hosts (Eadington and Nashar, 1978).
246 Nevertheless, topaz is a frequent greisen mineral and in granites it has often been considered a sub-
247 solidus replacement phase linked to autometasomatic processes, i.e. to alteration by the last water-
248 rich fluid trapped within the rock, or to external fluids (Manning and Exley, 1984; Kleeman, 1985).
249 Sometimes, it is developed in miarolitic cavities of granites and pegmatites as a late vapour phase
250 (e.g.; Williamson et al., 1997; Colombo et al., 2009).
251
252 *6.1 Textural and compositional evidence for a primary crystallization of topaz in the Chivinar*
253 *rhyolite*

The topaz crystals in the Chivinar rhyolitic lavas show different modes of occurrence. Two of these suggest igneous textural relationships: (a) in correspondence of concentration of voids, topaz forms anhedral/subhedral grains in association with quartz (Fig. 4C-G); (b) scattered in the matrix, topaz forms glomeroporphyritic elongate grains, again in association with quartz but without a noticeable concentration of voids. A third mode of occurrence (c) is within voids, where it shows idiomorphic terminations (Fig. 4F) indicating crystallization in fluid-filled cavities. Topaz is never associated to secondary minerals; indeed, the Chivinar rhyolites lack any evidence of replacement of primary minerals by secondary phases out of the alteration zone (i.e. no albite, sericite or topaz replacing plagioclase and alkali feldspar). White mica is frequently encountered in sample TG-9, but it is never found in replacement of feldspars; rather, it is interstitial in the groundmass, suggesting crystallization from the residual melt. Moreover, the miaroles in all the samples are never lined or filled by secondary phases. Thus, all topaz occurrences in the Chivinar rhyolite belong to the final phases of magmatic crystallization of the rhyolitic magma.

From the point of view of the chemical composition, the presence of magmatic topaz requires a fluorine-rich and peraluminous melt. Generally, in the final stages of differentiation, rhyolitic magmas may become volatile-rich, particularly in halogens. While chlorine tends to be characteristic of peralkaline rhyolites, fluorine (and a high F/Cl) is characteristic of peraluminous rhyolites (Scaillet and MacDonald, 2004; and references therein). Fluorine tends to remain in the silicate melt until late in the magma differentiation process, having a low $D_{fluid/melt}$ (0.15-0.04 is reported in peraluminous melts, see Baker and Alletti, 2012) and is not lost into the volatile phase until very low pressures (Aiuppa et al., 2009). Thus, the F content of the final Chivinar rhyolite melt was presumably very high, also in the presence of an exsolved aqueous phase. At this stage, the peraluminous composition of the Chivinar rhyolite and the subtraction of most Ca from melt by the former crystallization of plagioclase phenocrysts, favoured the crystallization of topaz in respect to

279 fluorite. Therefore, the chemistry of the Chivinar rhyolite is in agreement with the interpretation of
280 topaz as a primary, late magmatic phase.
281 Since topaz occurs in the groundmass, when it crystallized from the residual melt an aqueous fluid
282 phase was already exsolved. This is demonstrated by the presence of fluid inclusions in crystals,
283 also. The F vapour/melt partition coefficient depends on F abundance: concentrations as high as
284 ≥7–8 wt % F in melt will result in F preferentially partitioning into the fluid phase (Webster, 1990;
285 Carroll and Webster, 1994; Dolejš and Baker, 2007). Such high concentrations are not common in
286 nature, but could have been achieved in the very residual melt of the Chivinar rhyolite, allowing F
287 escape into the vapour phase. This explains how crystallization of topaz could continue into the
288 fluid-filled bubbles (Fig. 4F).
289
290 *6.2 Crystallization history of the Chivinar topaz rhyolites*
291
292 The composition of the Chivinar topaz rhyolite rocks, with very low Sr and Ba and high Rb and Nb,
293 indicates that the melt was highly differentiated. The low phenocryst content of the Chivinar
294 rhyolitic lavas suggests a low liquidus temperature, due to the presumably high F content of the
295 silicic melt. The presence of two feldspars in equilibrium indicates subsolvus crystallization, in
296 agreement with high P-fluid. The magmatic garnet with >20 wt% MnO indicates a relatively low
297 crystallization pressure, <300 MPa, according to experimental and geological reconstructions in
298 peraluminous plutons (Miller and Stoddard, 1981 and reference therein). Therefore, the storage
299 pressure of the rhyolitic magma can be assessed at 300-400 MPa.
300 The crystallization temperature in the magma chamber, estimated from the phenocrysts - oligoclase
301 and sanidine – composition, is 720-730°C for 4 wt% H_2O, according to the geothermometer of
302 Putirka (2008) for a pressure of 300-400 MPa. As a comparison, 775+40°C to 800°C were
303 calculated for Taylor Creek rhyolite, based on two feldspar equilibrium and the Fe-oxides

304 geothermometer (Duffield and Brey, 1990). The same authors estimated 700°C to 800°C for
305 crystals in miarolitic cavities of Taylor Creek lava.
306 Quartz, sanidine and plagioclase form the groundmass crystallizing assemblage, whose nucleation
307 was in response to magma ascent, decompression and fluid exsolution. The size, shape and mutual
308 relationships of the groundmass crystals, lacking the skeletal microlites indicative of high
309 undercooling, suggests a moderate nucleation rate, as well as moderate growth rate in response to a
310 rather slow cooling of the interior of the domes. Exsolution of an aqueous fluid, evidence of which
311 remains in the abundant primary fluid inclusions in the late groundmass crystals (particularly in
312 topaz) and in the trails of secondary fluid inclusions in the phenocrysts (Fig. 4A), began early
313 during magma ascent, but was important at the late stage of groundmass crystallization. The
314 absence of glass and of devitrification textures is in agreement with the low viscosity of the final F-
315 rich melt, allowing element diffusion and complete groundmass crystallization during the final
316 stages of cooling of the lava domes. The isotropic texture of the rocks indicates that crystallization
317 took place without flowing of magma, that is after the dome emplacement.
318 During the slow cooling above the solidus, crystallization of the groundmass crystals (quartz,
319 sanidine, sodic plagioclase) forced the melt composition to a very residual chemistry. The F-rich
320 and low-viscosity interstitial melt could migrate through the microlite framework (Fig. 8), in a
321 similar way to the gas filter-pressing process forming segregation vesicles in basaltic dykes
322 (Sanders, 1986). This mechanism permitted the formation of the quartz+topaz+vapour bubbles
323 concentrations, similar to the miaroles that form in felsic fine-grained intrusions crystallizing at
324 shallow crustal levels (Fig. 8). This was because the composition of the local residual magma
325 attained high fluorine content, resulting in moving the eutectic composition and enlarging the quartz
326 field. The residual melt at this point was probably of topazite, rather than ongonite, composition
327 (i.e.; Kortemeier and Burt, 1988), and the fluorine content was high enough to allow F partitioning
328 into the vapour phase and crystallization of vapour-phase topaz (Fig. 8).

329 The fact that the miaroles have irregular shapes, controlled by the crystals already present in the
330 groundmass, is in agreement with their formation during a late stage release of volatiles (Vernon,
331 2004; Agangi et al., 2010). Besides topaz, quartz and sporadic other minerals concluded their
332 crystallization in the fluid-filled vesicles by precipitation from the vapour phase (Candela and
333 Blevin, 1995) (Fig. 8).
334 The rounded shape shown by quartz crystals in the groundmass may be due to the high volatile
335 content of the final interstitial melt, inhibiting crystallization. Alternatively, taking into account that
336 quartz shows resorption while feldspars do not, and that the field of stability of quartz was
337 expanded at the expenses of feldspars by the presence of fluorine, we propose that the
338 crystallization of topaz, decreasing fluorine in melt, may have resulted in quartz instability causing
339 the rounded corners. Resorption of early quartz crystals in silicic systems may be caused by
340 adiabatic decompression, also, as proposed in several recent studies (e.g. Agangi et al., 2011), but
341 this mechanism is not suitable to explain the texture of the Chivinar rhyolites. In the Chivinar
342 domes, rounding affects groundmass quartz microlites in the inner dome portion, therefore it
343 occurred after dome emplacement; decompression of the partially molten dome interior after dome
344 emplacement, possibly provoked by carapace brecciation episodes, would result in rapid microlite
345 nucleation and growth in the residual melt, originating a texture completely different from that
346 observed.
347 Cooling of the dome interior continued slowly below the solidus. The Na-rich lamellae in alkali
348 feldspar crystals could represent exsolution lamellae due to feldspar unmixing, indicating that
349 cooling below the solidus was sufficiently slow to allow cryptoperthite development (Fig. 4G). On
350 the other hand, it cannot be excluded that the Na-rich lamellae indicate incipient albitization of
351 sanidine in the presence of a Na-bearing fluid. In this hypothesis, albitization would represent a late,
352 autometasomatic process in the interior of the dome. The discrimination between the two processes
353 is complicated by the fact that albitization develops along the same planes of perthitic textures

354 (Norberg et al., 2011). However, even if any albitization may have occurred, it must have been an
355 incipient process without noticeable consequences on the rock composition.
356
357 *6.3 Rare metals minerals*
358
359 Accessory minerals in the Chivinar rhyolites account for their high content in Nb and Ta, and this is
360 in agreement with the chemistry of the lavas. For instance, Nb-bearing rutile is one of the main
361 accessories found in the heavy mineral fraction, and the partition coefficients DNb and DTa
362 between rutile and melt for peraluminous magmas with ASI=1.22, the same of the Chivinar
363 rhyolite, are reported to be close to 4900 and 1900, respectively (Linnen and Keppler, 1997). The
364 accessories are sometimes found inside phenocrysts (Fig. 4B) but they are often interstitial in the
365 groundmass or even in correspondence of the vesicles. This indicates that they crystallized also
366 from the final residual melt+vapour phase. This behaviour, already reported in volatile-rich silicic
367 magmas (Agangi et al., 2010), supports a role of F-rich fluids in transporting immobile elements
368 such as Nb and Ta.
369 The data collected so far indicate the existence, in Late Miocene, of a F-H_2O-rich and rare metal-
370 rich magma chamber feeding the silicic Chivinar volcanic phase. This suggests that rare metals
371 mineralizations formed in the Chivinar region (René and Škoda, 2011). The extent of the
372 mineralization depends, besides the extent of the silicic magma system after the rhyolitic lava
373 effusion, on the timing and extent of F partitioning in the fluid phase and of Nb and Ta entering
374 accessories. The secondary mineralogy present in the Chivinar rocks, dominated by Nb-Ta-Mn
375 oxides and silicates and devoid of chalcophile elements, and the fact that alteration affects only the
376 rhyolitic rocks and not the younger andesite sequence, suggests a genetic link of the alteration
377 mineralogy with the topaz rhyolite magmatic system, rather than with an andesitic one.
378
379 *6.4 Geodynamic setting*

In addition to the Central Andes, rhyolitic lavas with magmatic topaz have been previously found in the western United States and Mexico, in the Basin and Range Province (Burt et al., 1982; Christiansen et al., 1983, 1986, 2007), and in the Nanling Range, in southern China (Xie et al., 2013). A common feature of these provinces is the presence of lithospheric extension in an intraplate setting, with crust-mantle interaction having an important role in the generation of the magmas. Magmatism in these provinces consisted of the intrusion of hot mafic magmas at the base and within the crust, providing a heat source for partial melting. Very similar tectono-magmatic conditions are found also for the topaz rhyolites of Chivinar, in the Central Andes. Even though Chivinar lies at the edge of the N-S trending volcanic arc of the Central Andes, its main structures are the WNW-ESE transtensive faults associated with the transverse COT structure. This suggests that, from a structural point of view, rhyolitic volcanism of Chivinar may be mostly related to the back-arc transtensive conditions of COT (Acocella et al., 2011), rather than to the arc structures. In fact, even though the overall tectonic setting of the Central Andes is contractional, transtensive or extensional conditions are found along the NW-SE trending fault zones in the back-arc (e.g. Riller et al., 2001). Among these is the transtensive COT, possibly carrying most of the extension in the Central Andes (Acocella et al., 2011). In this context, the compositional features of the Chivinar topaz rhyolites, in particular the high Nb-Ta and low Y/Nb (Fig. 6), could indicate partial melting of a continental crust previously intruded by mafic igneous bodies in an extensional regime, similarly to the North America topaz rhyolites (Christiansen et al., 2007). Therefore, despite the overall contractional or strike-slip setting of the arc, it is interesting to underline a connection between the transtensive/extensional features of the COT and intraplate extensional settings elsewhere. These similarities highlight preferred conditions for the formation of magmatic topaz.

7. Conclusions

The late magmatic origin of topaz in the Chivinar rhyolite lavas is supported by its igneous textural relationships with magmatic crystals and is in accordance with the peraluminous composition of the rhyolites. In addition, the topaz lacks any evidence of relationships with post-emplacement hydrothermal alteration. Textural evidence indicates that the phenocryst-poor lava of the domes interior underwent very slow cooling, and final crystallization took place in a large temperature interval. During the crystallization of the quartz-feldspathic groundmass, we propose that the F-rich, low-viscosity residual melt migrated in the crystal network and was concentrated, forming miaroles in which an assemblage topaz+quartz+vapour bubbles formed. In this final stage of groundmass crystallization, the F content in melt was so high that F could escape into the vapour phase, allowing also the final crystallization of topaz in the fluid-filled vesicles.

Given the magmatic origin of topaz, the topaz-bearing mineral assemblage in the Chivinar rhyolites suggests the existence of F-rich and rare metals-rich Late Miocene magma chambers. In addition, the alteration dominated by Nb-Ta-Mn oxides and silicates, affecting localized areas of the rhyolitic domes and pre-dating the following andesitic phase of the Chivinar volcano, suggests a genetic link with the topaz rhyolite magmatic system. This raises the possibility of the existence of veins or replacement deposits of rare metals, as well as of rare metals pegmatite bodies, in the Chivinar area. The extensional regime due to the presence of the transtensive COT structure suggests a correspondence with topaz rhyolites in North America and China, sharing similar geochemical features unrelated to subduction, and, thus highlights preferred conditions for the formation of magmatic topaz in overall intraplate settings.

Acknowledgements

The authors thank two anonymous reviewers for their comments and suggestions. This work has been carried out in the framework of the scientific convention between Pisa (Italy) and Salta (Argentina) Universities. The research was supported by the FONCYT-AGENCIA, (PICT Nº 0745 project), Salta University Research Council (CIUNSA-Project Nº 1861) and University of Pisa funds.

References

Acocella, V., Gioncada, A., Omarini, R., Riller, U., Mazzuoli, R., Vezzoli, L., 2011. Tectonomagmatic characteristics of the back-arc portion of the Calama-Olacapato-El Toro Fault Zone, Central Andes. Tectonics 30 TC3005 doi:10.1029/2010TC002854.

Agangi, A., Kamenetsky, V., McPhie, J., 2010. The role of fluorine in the concentration and transport of lithophile trace elements in felsic magmas: Insights from the Gawler Range Volcanics, South Australia. Chemical Geology 273, 314–325.

Agangi, A., McPhie, J., Kamenetsky, V.S., 2011. Magma chamber dynamics in a silicic LIP revealed by quartz: the Mesoproterozoic Gawler Range Volcanics. Lithos 126, 68-83.

Aiuppa, A., Baker, D.R., Webster, J.D., 2009. Halogens in volcanic systems. Chemical Geology 263, 1-18.

Baker, D.R., Alletti, M., 2012. Fluid saturation and volatile partitioning between melts and hydrous fluids in crustal magmatic systems: The contribution of experimental measurements and solubility models. Earth-Science Reviews 114, 298-324. DOI :10.1016/j.earscirev.2012.06.005.

Blasco, G., Zappettini, E.O., Hongn, F., 1996. Hoja geológica 2566−1, San Antonio de los Cobres, Programa Nac. de Carteas Geol. de la Repub. Argentina, Dirección. Nacional del Servicio Geológico, Buenos Aires, Argentina.

Breiter, K., 2012. Nearly contemporaneous evolution of the A- and S-type fractionated granites in the Krušné hory/Erzgebirge Mts., Central Europe. Lithos 151, 105-151.

457 Burt, D.M., Sheridan, M.F., Bikun, J.V., Christiansen, E.H. 1982. Topaz rhyolites: distribution,
458 origin, and significance for exploration. Economic Geology 77, 1818-1836.
459 Candela, P.A., Blevin, P.L., 1995. Do some miarolitic granites preserve evidence of magmatic
460 volatile phase permeability?. Economic Geology 90, 2310-2316.
461 Carroll, M.R., Webster, J. D., 1994. Solubilities of sulfur, noble gases, nitrogen, chlorine, and
462 fluorine in magmas Reviews in Mineralogy and Geochemistry 30, 231-279.
463 Christiansen, E.H., Burt, D.M., Sheridan, M.F., Wilson, R.T., 1983. The petrogenesis of topaz
464 rhyolites from wester united states. Contributions to Mineralogy and Petrology 83, 16-30.
465 Christiansen, E.H., Burt, D.M., Sheridan, M.F., 1986. The geology of topaz rhyolites from the
466 western United States. Geological Society of America Special Paper, 205, 82 pp.
467 Christiansen, E.H., Haapala, I., Hart, G.L. 2007. Are Cenozoic topaz rhyolites the erupted
468 equivalents of Proterozoic rapakivi granites? Examples from the western United States and
469 Finland. Lithos 97, 219-246.
470 Colombo, F., Lira, R., Pannunzio Miner, E.V., 2009. Mineralogical characterization of topaz from
471 miarolitic pegmatites and W-bearing greisen in the A-type El Portezuelo Granite, Papachacra
472 (Catamarca Province). Revista Asociación Geológica Argentina 64 (2), 194-200.
473 Dolejš, D., Baker, D.R., 2007. Liquidus equilibria in the system K_2O–Na_2O–Al_2O_3–SiO_2–F_2O1–
474 H2O to 100 MPa: II. Differentiation paths of fluorosilicic magmas in hydrous systems. Journal
475 of Petrology 48 (4), 807-828.
476 Eadington, P. J., Nashar, B., 1978. Evidence for the Magmatic Origin of Quartz-Topaz Rocks From
477 the New England Batholith, Australia. Contribution Mineralogy and Petrology 67, 433-438.
478 Duffield, W.A., Brey, E.A., 1990. Temperature, size, and depth of the magma reservoir for the
479 Taylor Creek Rhyolite, New Mexico. American Mineralogist 75, 1059-1070.
480 Huspeni, J.R., Kesler, S.E., Ruiz, J., Tuta, Z., Sutter, J.F., Jones, L.M., 1984. Petrology and
481 geochemistry of rhyolites associated with tin mineralization in northern Mexico. Economic
482 Geology 79, 87-105.

Irvine, T.N., Baragar, W.R.A., 1971. A guide to chemical classification of the common rocks. Canadian Journal of Earth Science 8, 523-548.

Johannes, W., Holtz, F., 1996. Petrogenesis and Experimental Petrology of Granitic Rocks, Springer-Verlag, Berlin, 335 pp.

Jordan, T.E., Alonso, R.N., 1987. Cenozoic stratigraphy and basin tectonics of the Andes Mountains 20º-28º South Latitude. The American Association of Petroleoum Geologists Bulletin 71, 49-64.

Keppler, H., 1993. Influence of fluorine on the enrichment of high field strength trace elements in granitic rocks. Contribution to Mineralogy and Petrology 114, 479-488.

Kleeman, J. D., 1985. Origin of disseminated wolframite-bearing quartz-topaz rock at Torrington, New South Wales, Australia. High-Heat Production (HHP) Granites, Hydrothermal Circulation and Ore Genesis. London, Institution of Mining and Metallurgy, 197-201.

Kortemeier, W.T., Burt, D.M., 1988. Ongonite and topazite dikes in the Flying W ranch area, Tonto basin, Arizona. American Mineralogist 73, 507-523.

Koukharsky, M., Munizaga, F., 1990. Los volcanes Guanaquero, Chivinar, Tul Tul, Del Medio y Pocitos, provincia de Salta, Argentina. Litología y edades K/Ar. XI Congreso Geologico Argentino, San Juan, Actas 1, 64-67.

Koukharsky, M., Pereyra, F., Etcheverria, M, Lanes, S., 1991. La riolita con topacio del cerro Chivinar, Departamento Los Andes, Provincia de Salta. Revista Asociacion Geologica Argentina 46, 349-351.

Le Bas, M.J., Le Maitre, R.W., Streckeisen, A., Zanettin, B., IUGS Subcommission on the Systematics of Igneous Rocks, 1986. A Chemical Classification of Volcanic Rocks Based on the Total Alkali-Silica Diagram. Journal of Petrology 27, 745-750.

Linnen, R.L., Keppler, H., 1997. Columbite solubility in granitic melts: consequences for the enrichment and fractionation of Nb and Ta in the Earth's crust. Contributions to Mineralogy and Petrology 128, 213-227.

509 Lukkari, S., 2002. Petrography And Geochemistry Of The Topaz-Bearing Granite Stocks In
510 Artjärvi And Sääskjärvi, Western Margin Of The Wiborg Rapakivi Granite Batholith. Bulletin
511 Of The Geological Society Of Finland 74 (1–2), 115–132.
512 Manning, D.A.C., Exley, C.S., 1984. The origins of late-stage rocks in the St Austell granite—a re-
513 interpretation. Journal of the Geological Society of London 141, 581-591.
514 Matteini, M., Mazzuoli, R., Omarini, R., Cas, R., Maas, R., 2002. The geochemical variations of the
515 upper cenozoic volcanism along the Calama–Olacapato–El Toro transversal fault system in
516 central Andes (~24°S): petrogenetic and geodynamic implications. Tectonophysics 345, 211-
517 227.
518 Miller, C.F., Stoddard, E.F., 1981. The role of manganese in the paragenesis of magmatic garnet: an
519 example from the old Woman-Piute range, California. Journal of Geology 89: 233-246.
520 Norberg, N., Neusser, G., Wirth, R., Harlow, D., 2011. Microstructural evolution during
521 experimental albitization of K-rich alkali feldspar. Contribution to Mineralogy and Petrology
522 162, 531-546.
523 Morimoto, N., 1988. Nomenclature of pyroxenes. Mineralogical Magazine 52, 535-55.
524 Orlandi, P., Gioncada, A., Vezzoli, L., Omarini, R., Mazzuoli, R., Lopez-Azarevich, V., Sureda, R.,
525 Azarevich, M., Bianchi, D., Acocella, V., Rusch, J., Guillou, H., Nonnotte, P., 2011. The topaz-
526 bearing rhyolite lavas from Chivinar volcanic complex (24°17’38’’S - 67°25’28’’W, Central
527 Andes, NW Argentina). 1er Simposio sobre petrología ígnea y metalogénesis asociada. San
528 Miguel de Tucumán, November 16-18, 2011.
529 Putirka, K., 2008. Thermometers and Barometers for Volcanic Systems. In: Putirka, K., Tepley, F.
530 (Eds.), Minerals, Inclusions and Volcanic Processes, Reviews in Mineralogy and Geochemistry,
531 Mineralogical Soc. Am., 69, 61-120.
532 René, M., Škoda, R., 2011. Nb-Ta-Ti oxides fractionation in rare-metal granites: Krásno-Horní
533 Slavkov ore district, Czech Republic. Mineralogy and Petrology 103, 37–48. DOI
534 10.1007/s00710-011-0152-z.

Riller, U., Petrinovic, I., Ramelow, J., Strecker, M., Oncken, O., 2001. Late Cenozoic tectonism, collapse calderas and plateau formation in the Central Andes. Earth Planetary Science Letters, 188, 299-311.

Rodríguez-Ríos, R., Aguillón-Robles, A., Leroy, J. L., 2007. Evolución petrológica y geoquímica de un complejo de domos topacíferos en el Campo Volcánico de San Luis Potosí (México). Revista Mexicana de Ciencias Geológicas 24 (3), 328-343.

Salfity, J.A., 1985. Lineamentos transversales al rumbo andino en el noroeste argentino. In: Actas IV Congreso Geológico Chileno, Antofagasta, Chile, 2, 119–137.

Sanders, I.S., 1986. Gas filter-pressing origin for segregation vesicles in dykes. Geological Magazine 123, 67-72.

Scaillet, B., Macdonald, R., 2004. Fluorite stability in silicic magmas. Contributions to Mineralogy and Petrology 147, 319–329.

Sinclair, W.D., 1986. Early Tertiary topaz rhyolites and associated mineral deposits in the northern Canadian Cordillera; products of anorogenic magmatism. Program with abstracts — Geological Association of Canada. Mineralogical Association of Canada Annual Meeting, 11, 127–128.

Sun, S., McDonough, W.R., 1989. Chemical and isotopic systematics of oceanic basalts: implications for mantle composition and processes. In Saunders, A. D. & Norry, M. J. (eds), 1989, Magmatism in the Ocean Basins, Geological Society Special Publication 42, 313-345.

Taylor, R.P., 1992. The petrological and geochemical characteristics of the Pleasant Ridge zinnwaldite-topaz granite, southern New Brunswick, and comparisons with other topaz-bearing felsic rocks. The Canadian Mineralogist 30, 895-921.

Taylor, R., 2009. Ore textures - Recognition and interpretation. Springer-Verlag, 282 pag., ISBN 978-3-642-01782-7.

Taylor, R.P., Fallick, A.E., 1997. The evolution of fluorine-rich felsic magmas: source dichotomy, magmatic convergence and the origins of topaz granite. Terra Nova 9 (3), 105-108.

560 Tuttle, O.F., Bowen N.L. 1958. Origin of Granite in the Light of Experimental Studies in the
561 System $NaAlSi_3O_8$-$KAlSi_3O_8$-SiO_2-H_2O. Geological Society of America 74, 153 p.
562 Vernon, R.H., 2004. A Practical Guide to Rock Microstructure. Cambridge University Press.
563 Webster, J.D., 1990. Partitioning of F between H_2O and CO_2 fluids and topaz rhyolite melt
564 Implications for mineralizing magmatic-hydrothermal fluids in F-rich granitic systems
565 Contributions to Mineralogy and Petrology 104, 424-438.
566 Whalen, J.B., Currie, K.L., Chappell, B.W., 1987. A-type granites; geochemical characteristics,
567 discrimination and petrogenesis. Contributions to Mineralogy and Petrology 95, 407–419.
568 Williamson, B.J., Stanley, C.J., Wilkinson, J.J., 1997. Implications from inclusions in topaz for
569 greisenisation and mineralisation in the Hensbarrow topaz granite, Cornwall, England.
570 Contributions to Mineralogy and Petrology 127, 119-128.
571 Xie, L., Wang R., Chen, J., Zhu, J., Zhang, W., Lu, J., Zhang, R., 2013. A tin-mineralized topaz
572 rhyolite dike with coeval topaz granite enclaves at Qiguling in the Qitianling tin district,
573 southern China. Lithos 170, 52–268.
574

575 Figure captions

576 Fig. 1. Geological framework of the Chivinar volcanic complex. (A) Location of the studied area
577 with respect of the morpho-structural units of the Central Andes. The Western Cordillera is the
578 active magmatic arc. Miocene to Quaternary volcanism develops in the backarc along some
579 transverse NW-trending lineaments as the Calama-Olacapato-El Toro (COT) fault system. (B)
580 Regional geologic map of the Puna plateau showing the location of the Chivinar volcano at the
581 boundary between the magmatic arc and backarc. SAC: San Antonio de los Cobres. (C)
582 Geologic map of the Chivinar volcano based on our new field mapping. Location of the samples
583 studied is shown.

584 Fig. 2. Fig. 2. Field photos of volcanic features of the Cerro Chivinar volcanic complex. Location of
585 the studied samples is also shown. (A) The northern flank of the Cerro Chivinar shows three
586 superposed and distinct eruptive packages, from bottom: TR = topaz-bearing rhyolite lava
587 domes; Mb = dacite megabreccia and pumice deposits; Lc = andesite lava cone. The red line is
588 the trace of the major NW-SE striking transtensive fault (white circles indicate a sinistral
589 kinematics). (B) The western flank of the Cerro Chivinar shows the stratigraphic and intrusive
590 relationships between the topaz-bearing rhyolite lava domes (TR) and the Eocene-Miocene
591 sedimentary substratum (Rp = red pelites; Gy = gypsum). Af = alluvial fan. Red lines are the
592 traces of the major NW-SE transtensive (white circles indicate a sinistral kinematics) and NS
593 transpressive striking faults.

594 Fig. 3. Composition of feldspars of the topaz rhyolites reported in the ternary An (anorthite)-Ab
595 (albite)-Or (orthoclase) diagram. The composition of the primary feldspars of the rhyolitic lavas
596 in the alteration zone is also reported.

597 Fig. 4. Petrographic thin section photos with crossed nicols (A, B) and backscattered electrons SEM
598 images (C…J) of Chivinar topaz rhyolite samples. A. Fluid inclusions trails in plagioclase
599 phenocryst (arrow shows an example). B. Sanidine phenocryst and zircon, xenotime accessories
600 in the holocrystalline, equant, quartz-feldspathic groundmass. C. Topaz concentration with

voids. D. Cryptoperthitic lamellae in alkali feldspar in the topaz rhyolite, testifying the final slow cooling phase of the lava dome; note the homogeneous core, representative of a former crystallization step at higher temperature. E. Zircon in void, in epitaxis with xenotime. F. Topaz, with syntaxial growth. G. Textural relationships between topaz and quartz (arrow indicates quartz-topaz contact). Note the frequent fluid inclusions in topaz. H. Di-octahedral mica flakes in the groundmass of Chivinar rhyolites, sample TG-9. I. Detail of veinlet in Chivinar rhyolite. Secondary minerals in vein are Mn-bearing amphiboles and Nb-bearing oxide. J. Detail of the rhyolite hosting veinlet in I: note the disseminated Nb-Ta-Ti oxides, compared to the rhyolite lava in C.

Fig. 5. A. Composition of the Chivinar rhyolites (open circles) reported in the TAS diagram (total alkali vs. silica, le Bas et al., 1986) and compared with the fields for topaz rhyolites from Christiansen et al. (2007) (light grey) and from Rodríguez-Ríos et al. (2007) (dark grey); the dashed line divides alkaline and subalkaline rocks after Irvine and Baragar (1971). The Chivinar andesitic rocks are also reported as black dots. B. Rare Earth Element patterns of the Chivinar topaz rhyolites normalized to chondrite after Sun and MacDonough (1989). Symbols and fields as in Figure 5A. C. Multielement spiderdiagrams of the Chivinar topaz rhyolites normalized to Primitive Mantle after Sun and MacDonough (1989). Symbols and fields as in Figure 5A.

Fig. 6. Chivinar topaz rhyolites plotted in the discrimination diagram for intraplate setting after Whalen et al. (1987). Open circles are Chivinar topaz rhyolites from this work (the two samples nearly coincide); light grey field is topaz rhyolites from Christiansen et al. (2007), white field is from Rodríguez-Ríos et al. (2007), dark grey field is from Xie et al. (2013).

Fig. 7. The "granite" system (Qz–Ab–Or) with the composition of Chivinar topaz rhyolite rocks (open circles). The solid line indicates the quartz–feldspar cotectic and the minimum melt composition at 1 kbar, H_2O-saturated conditions (Tuttle and Bowen, 1958). The arrow shows the eutectic variation for F added to the haplogranite composition (Johannes and Holtz, 1996;

and references therein). Grey field is topaz rhyolites from Christiansen et al. (2007) and white field is topaz granites from Taylor and Fallick (1997).

Fig. 8. Conceptual model of formation of the topaz+quartz+voids association in the Chivinar rhyolite.

Table captions

Table 1. Representative EDS analyses of primary minerals in the Chivinar rhyolitic lavas.

Table 2. Representative EDS analyses of secondary minerals in the Chivinar altered rhyolitic lavas.

Table 3. A. Whole rock major element composition and CIPW norm of the analyzed Chivinar rocks. ASI: Alumina Saturation Index, molecular $[Al_2O_3]/[CaO]-1.67*[P_2O_5]+[Na_2O]+[K_2O]$. B. Trace element composition of the Chivinar topaz rhyolites.

Topaz magmatic crystallization in rhyolites of the Central Andes (Chivinar volcanic complex, NW Argentina): constraints from texture, mineralogy and rock chemistry

Gioncada Anna[a], Orlandi Paolo[a], Vezzoli Luigina[b], Omarini Ricardo H.[c], Mazzuoli Roberto[a], Lopez-Azarevich Vanina[c], Sureda Ricardo[c], Azarevich Miguel[c], Acocella Valerio[d], Ruch Joel[d]

[a] *Dipartimento di Scienze della Terra, Università degli Studi di Pisa, Pisa, Italy*

[b] *Dipartimento di Scienza e Alta Tecnologia, Università dell'Insubria, Como, Italy*

[c] *Facultad de Ciencias Naturales, Universidad Nacional de Salta, CEGA-CONICET Salta, Argentina*

[d] *Dipartimento di Scienze, Università Roma Tre, Roma, Italy*

Corresponding author: A.Gioncada gioncada@dst.unipi.it

Abstract: Topaz-bearing rhyolite lavas were erupted as domes and cryptodomes during the early history of the Late Miocene Chivinar volcano, in Central Andes. These are the only topaz rhyolite lavas recognized in Central Andes. Textural, mineralogical and geochemical data on the Chivinar rhyolites suggest that topaz crystallized from strongly residual, **fluorine**-rich, peraluminous silicate melts of topazite composition before the complete solidification of the lava domes. Crystallization of the rhyolitic magma began with sodic plagioclase and alkali feldspar phenocrysts in the magma chamber, followed by groundmass quartz+alkali feldspar+minor sodic plagioclase during dome emplacement, and terminated with quartz+topaz+vapour bubbles forming small scattered miaroles. Fluorine partitioning **into** the fluid phase occurred only in the final stage of groundmass crystallization. The magmatic origin of topaz indicates the presence of a **fluorine**-rich highly differentiated magma in the early history of the Chivinar volcano and suggests the possibility of rare metals mineralizations related to the cooling and solidification of a silicic magma chamber. A late fluid circulation phase, pre-dating the andesitic phase of the Chivinar volcano, affected part of the topaz rhyolite lavas. The presence of Nb, Ta and Mn minerals as primary accessories in the rhyolites and as secondary minerals in veins suggests a connection of the fluid circulation phase with the silicic magmatic system. Although at the edge of the active volcanic arc, the Chivinar topaz rhyolites are in correspondence of the transtensive Calama-Olacapato-El Toro fault **system**, suggesting preferred extensional conditions for the formation of magmatic topaz in convergent settings**, consistently with evidence from other known cases worldwide.**

Key words: Topaz-bearing rhyolite, fluorine, magmatic volatiles, miarolitic texture, Central Andes

1. Introduction

Although more frequently interpreted as the product of post-magmatic vapour-phase alteration (e.g.; Taylor, 2009), topaz is also a rare primary constituent of magmatic rocks, originated by the crystallization of peraluminous and fluorine-rich silicic magmas (Scaillet and MacDonald, 2004; Lukkari, 2002; Agangi et al., 2010). The silicatic melts enriched in fluorine have particular physical properties, i.e. low viscosity and density (Aiuppa et al., **2009**). These enhance the efficiency of the petrogenetic processes, allowing segregation of unusually low fractions of partial melt from the source, as well as favouring crystal-melt fractionation during magma ascent. By that, **fluorine (F)** promotes the production and release of very small volumes of felsic magma enriched in a wide variety of incompatible elements (Keppler, 1993) and, consequently, potentially related to economically interesting ore mineralizations (e.g.; Burt et al., 1982; Xie et al., 2013).

In this paper we report the occurrence and the mineralogical, petrographic and chemical characteristics of rhyolitic lavas bearing topaz from the Late Miocene Chivinar volcano, located in Central Andes (Fig. 1; Koukharsky et al., 1991; Orlandi et al., 2011). While several high-silica, topaz-bearing rhyolitic lavas of Cenozoic age have been recognized **in North America (western United States and Mexico;** Christiansen et al., 1986; Huspeni et al., 1984; Sinclair, 1986; Rodríguez-Ríos et al., 2007), the Chivinar topaz rhyolites are, to date, the only occurrence in the Andes of South America.

Owing to their location at the intersection of the Andean active magmatic arc with a major NW-striking fault system (Fig. 1A) and to their peculiar mineralogy, the Chivinar rocks present a two-fold interest. First, the knowledge of the petrogenetic processes responsible for the composition of these lavas may add new elements for the interpretation of the genesis and evolution of magmas at the arc-back-arc boundary in Central Andes (Matteini et al., 2002; Acocella et al., 2011). Second, understanding the origin of topaz in magmatic rocks may contribute to explain mineralizations in rare, economically interesting elements (Xie et al., 2013 and references therein). For both purposes,

the determination of the primary (magmatic) vs. secondary (hydrothermal) origin of topaz is crucial. This contribution presents the textural, mineralogical and geochemical constraints to the magmatic origin of topaz in the Chivinar rhyolite and proposes a model for the magmatic crystallization of topaz rhyolite.

2. Geological framework

Cerro Chivinar is a Miocene volcano located in the western Puna plateau of the Central Andes (24º14'S – 67º27'W; 5125 m above sea level, a.s.l.), at the intersection between the N-S trending active magmatic arc (Western Cordillera) and the NW-SE trending Calama-Olacapato-El Toro (COT) transtensive fault zone (Salfity, 1985; Acocella et al., 2011) (Figs. 1A and 1B). The COT fault zone coincides with a well-defined volcanic belt, consisting of stratovolcanoes, lava domes and some monogenetic scoria centres and formed in the last 15 Ma. The composition of the magmas erupted along the COT volcanic belt includes calcalkaline magmas ranging from basaltic andesites to dacites and rhyolites, and shoshonitic magmas erupted at the mafic monogenetic scoria centres (Acocella et al., 2011 and references therein).

The geology of the Chivinar volcano has been never described in detail. The main geological features were formerly sketched in Koukharsky and Munizaga (1990) and Koukharsky et al. (1991), reporting the occurrence of topaz in the rhyolitic lavas of the volcano. Our new geologic field mapping shows that Chivinar is a polygenetic volcanic complex built by three superposed and distinct eruptive packages (**Figs. 1C and 2A**). The oldest unit is made up of a cluster of topaz rhyolite lava domes exposed on the N and W basal platform of the volcano, between 3500 and 4000 m a.s.l.. The following unit consists of radially emplaced coarse dacite breccia and pumice deposits that resulted from lava dome catastrophic destruction events. Finally, an andesite lava cone caps the volcanic edifice. A K/Ar age of 9.0±0.4 Ma was determined on andesite of the Chivinar lava cone

(Koukharsky and Munizaga, 1990). The substratum of the volcano is represented by continental terrigenous and evaporitic deposits of Late Eocene-Miocene age (Fig. 1B; Geste, Pozuelos and Sijes Formations; Jordan and Alonso, 1987; Blasco et al., 1996). The most active tectonic systems are WNW-ESE trending transtensive and extensional faults (**Figs. 1 and 2**), similarly to the ones found along the eastern continuation of the COT (Acocella et al., 2011). These systems seem also to control the preferred WNW-ESE elongation of the volcano.

The Chivinar topaz rhyolites consist of a group of coalescent lava domes that were extruded as small, endogenous lava domes and shallowly emplaced intrusive domes and plugs (Fig. 1C). The lava emplacement lacks **of** associated explosive products. Field evidence excludes the association of the rhyolite with one or more caldera structures. Rhyolite rests directly on or intrudes the Eocene-Miocene sedimentary substratum **(Fig. 2B)**. Intrusive and cooling histories of individual lava bodies are locally constrained by lava textures, as marginal vitrophyres, flow-banding and breccias, at the contact with host sediments. The **remnant** domes range from 0.3 to 1 km in diameter and are up to 250 m high. The rhyolite dome field makes up nearly one third of the volume of the Chivinar complex.

At the end of the oldest Chivinar eruptive episode, the rhyolite lavas were intensely deformed, eroded and altered. The pervasiveness of the deformation and hydrothermal alteration contrasts with the fresh younger breccias and lavas that make up the rest of the edifice, suggesting that tectonism and fluid circulation followed by exogenous weathering occurred prior to renewed construction of the edifice.

3. Sampling and analytical methods

Three samples of the rhyolitic domes showing no **macroscopic** evidence of alteration were selected for the preparation of polished thin sections and for crushing and powdering. TG-9 rhyolite

represents the external part of a dome near the contact with the host evaporitic rock; TG-10 and TG-16 come from the inner part of the coalescent dome cluster (**Figs. 1C and 2**). Also, three samples of the rhyolites were collected from outcrops showing hydrothermal alteration evidence, to evaluate the relationships between the primary and secondary mineralogy. Finally, representative samples of the Chivinar dacites and andesites capping the volcanic edifice were selected for comparing the major elements composition with the silicic lavas.

Whole-rock X-ray fluorescence (XRF) analyses of major oxides were done on fused samples with an ARL 9400 XPp instrument at the Dipartimento di Scienze della Terra, University of Pisa, Italy. Accuracy is 4–7% for concentrations <1 wt%, 2–4% for concentrations 1–10 wt%, 1% for concentrations >10 wt%. Trace-element analyses and Loss on Ignition determinations were carried out on powdered rock samples at Acme Laboratories, Ontario, Canada.

Microanalytical data were collected on polished **and carbon-coated** rock sections with a Philips XL30 scanning electron microscope equipped with microanalysis EDAX (standard-less software DXi4) at Dipartimento di Scienze della Terra, University of Pisa, Italy (acceleration voltage 20 kV, beam current 5 nA, live time 100 s). The accuracy is better than 0.5% if abundance is >15 wt%, 1% if abundance is around 5 wt%, and better than 20% if abundance is around 0.5 wt%.

Mineral separations were carried out to investigate the heavy mineral fraction by means of SEM-EDS with the above described facilities. XRD analysis of selected mineral grains were carried out at Dipartimento di Scienze della Terra, University of Pisa with **a** Gandolfi camera (114.6 mm in diameter) and CuKα radiation.

4. Petrography and mineral chemistry

The Chivinar rhyolites are characterized by a very homogeneous white to creamy white colour. The hand samples show porphyritic texture, with about 10 % in volume of transparent phenocrysts, 0.5

to 3 mm in size, rare coloured minerals, <1 mm in size, and very fine voids. No xenocrysts nor xenoliths from the andesitic magmatic system have been found in the silicic lava samples.

The phenocrysts are plagioclase, consisting of euhedral stubby oligoclase with moderate direct zoning, and sanidine, with low 2V angle (15-20°), with elongated lath shape and lower size than plagioclase (Figs. **3 and 4A-B**; Table 1). In sample TG-9, oligoclase is the only phenocryst.

The groundmass of the Chivinar rhyolites is holocrystalline and shows a fine-grained (40-100 microns), isotropic granular texture, consisting of equant subidiomorphic quartz, alkali feldspar and sodic plagioclase **(Fig. 4B-C). The quartz microlites locally show rounded corners.**

Trails of minute vapour-rich secondary fluid inclusions cross-cutting phenocrysts are rather common (Fig. 4A). The groundmass crystals mainly host solid inclusions of accessory minerals and minute vapour-rich inclusions of primary formation.

Voids, mainly 50-200 microns in size, are disseminated in the lavas. The void boundaries are irregular, following the boundaries of the rock crystals, which sometimes protrude into the void.

The composition of plagioclase phenocrysts is quite constant, with modest direct zoning $An_{15}Ab_{79}$-$An_{10}Ab_{85}$, and the groundmass microlites have the same composition of the phenocryst's rims. The composition of alkali feldspar covers the range $Or_{65}Ab_{35}$-$Or_{51}Ab_{47}$ from phenocrysts to groundmass microlites (Fig. **3**). The alkali feldspar crystals in the groundmass show **subtle** lamellae of Na-rich feldspar, 0.5-1 microns thick (Fig. **4D), developing preferentially from the rim inward.**

The average volume proportions of quartz, plagioclase and alkali feldspar in the rocks are 36±2, 14±3 and 49±2 vol. %, respectively, determined with image analysis using microphotos and backscattered **e**lectrons SEM images (ImageJ version 1.42q). Several other minerals occur in <3 **vol.** % to trace amounts, including topaz, magnetite, both interstitial and included in quartz, ilmenite, a F-bearing tri-octahedral mica (montdorite/fluor-phlogopite; see Table 1), calcic amphibole, zircon and xenotime-Y. Zircon and xenotime-Y are **commonly included in** feldspar

phenocrysts (Fig. **4B). In addition, topaz, zircon and xenotime sometimes show crystallization with idiomorphic terminations in voids (Fig. 4E-F).**

Other accessories have been identified in the heavy mineral fraction (see below). In sample TG-9, **muscovite**-like di-octahedral mica minerals are disseminated as clusters of fine-grained flakes in the groundmass of the lava (Table 1**; Fig. 4H).**

Topaz is easily encountered in the samples TG-10 and TG-16, while it is sporadic in TG-9; it occurs in the matrix in association with quartz, or forms glomeroporphyric aggregates of acicular crystals as described in Arizona ongonites (Kortemeier and Burt, 1988). In samples TG-10 and TG-16 it concentrates in particular in correspondence of clusters of voids (e.g.; Fig. **4C-G**), with both allotriomorphic and idiomorphic crystals.

The heavy mineral concentrates of the Chivinar topaz-bearing samples reveal a variety of accessory minerals in the fraction with density higher than 2.9 g/cm^3, which represent between 1 and 2 wt% in the studied samples. The most abundant mineral phase is topaz, representing around 50% by weight of the heavy fraction (Fig. **4F)**, followed by a Nb-rich rutile variety. Monazite-(Ce), xenotime-(Y, REE), a**n** Fe-bearing tourmaline variety, zircon (with Th, U and Hf) and Mn-garnet (spessartine) are present in trace amounts. All these mineralogical phases have been identified by SEM-EDS semi-quantitative chemical analyses (Table 1). The content of Nb in the presumed rutile resulted remarkably high; therefore, the identification was confirmed by an X-ray powder pattern collected with **a** Gandolfi camera.

In the samples from the outcrops affected by hydrothermal alteration, the rhyolitic lavas **show the same primary mineralogy and texture of the unaltered samples. They** are porphyritic, with millimetric plagioclase and sanidine phenocrysts in a quartz-feldspathic groundmass. The secondary minerals are both disseminated and in veinlets that stand out for their dark green to black colour (Fig. **4I-J**) and include Mn-bearing silicates **(Mn-bearing sodic amphibole and sodic pyroxene),** Mn-bearing Fe-Ti oxides of the magnetite and ilmenite series, Mn-bearing apatite and Nb-Ta-bearing rutile (Table 2). Secondary alkali feldspar occurs in the host rock at the vein contact (Table

2). In some places, **instead, alteration resulted in complete leaching of feldspars and silicification, with the resultant rock composed of relict fine-grained quartz and scattered Nb-Ta-bearing rutile and secondary silica phases.**

The rocks of the Chivinar volcanic units following the rhyolitic lava domes are mainly andesitic lavas and minor pumiceous deposits. They are porphyritic, with phenocrysts of plagioclase and hornblende, minor orthopyroxene and scarce clinopyroxene, biotite and Fe-oxides in a groundmass made of the same mineral phases and a variable amount of glass. The least evolved andesite samples show abundant olivine phenocrysts with iddingsite rims.

5. Whole-rock major and trace element composition

The composition of the Chivinar topaz-bearing lavas falls in the TAS diagram in the rhyolite field, with a Na_2O+K_2O around 8 wt% (Fig. 5A) and $K_2O/Na_2O = 1$ (Table 3). The rhyolites with silica around 75-77 wt% are peraluminous and corundum appears in their CIPW norm, while the TG-9 rhyolite with 74 wt% SiO_2 is metaluminous. The composition of other volcanic rocks forming the Chivinar volcanic complex is remarkably different, ranging in silica from 59 to 63 wt% (Fig. **5A):** the pumice clasts in the pyroclastic breccias are dacites and the final lava flows are andesites, belonging to the high-K calcalkaline series.

A comparison of the Chivinar rhyolites with other topaz-bearing silicic rocks indicates similarly high Rb, Th, U, Pb, and Y but even higher Nb, Ta, while the LREE values are lower (e.g.; **Christiansen** et al., 1983; 1986; 2007; Lukkari, 2002; Rodríguez-Ríos et al., 2007) (Fig. **5B,** C). The REE patterns are notably flat, with $(La/Yb)_n = 2.5$, and display a strong Eu negative anomaly, with Eu/Eu* = 0.11 (Fig. **5B)**.

The Chivinar rhyolites have the same geochemical characteristics (P_2O_5 <0.1 wt%, Al_2O_3 <14.5 wt%, SiO_2 >73 wt%) of the low-P_2O_5 subtype of topaz-granites after Taylor and Fallick (1997), and

of low-P_2O_5 granites from Central Europe and Scandinavian described by Breiter (2012) and Lukkari (2002). The low P_2O_5 in the Chivinar topaz rhyolites is in agreement with the absence of apatite as accessory (all Ca contributed to plagioclase) and contributes to distinguish these silicic magmas from S-type peraluminous magmas, suggesting a derivation by partial melting of an igneous protolith rather than of a pelitic one. **In the discrimination diagram suggested by Whalen et al. (1987) for granites, the Chivinar topaz rhyolites fall in the field for intraplate settings (Fig. 6).** The North America topaz rhyolites show the same major elements characteristics and similarly high Nb content and Nb/Y value (Fig**. 6),** and are explained with melting of continental crust previously intruded by mafic magmas with an intraplate signature **(Christiansen et al., 2007; Rodríguez-Ríos et al., 2007).**

6. Discussion

Whether topaz has a late magmatic (primary) or hydrothermal (secondary) origin has been a matter of discussion for several silicic igneous complexes. There is abundant petrographic evidence for topaz having formed as a liquidus phase in many topaz granites (Taylor, 1992, Lukkari, 2002) and, also, in sub-volcanic rhyolites (Xie et al., 2013). Indeed, the occurrence of melt inclusions in topaz has been taken as a proof of a magmatic origin for topaz hosts (Eadington and Nashar, 1978). Nevertheless, topaz is a frequent greisen mineral and in granites it has often been considered a sub-solidus replacement phase linked to autometasomatic processes, i.e. to alteration by the last water-rich fluid trapped within the rock, or to external fluids (Manning and Exley, 1984; Kleeman, 1985). Sometimes, it is developed in miarolitic cavities of granites and pegmatites as a late vapour phase (e.g.; Williamson et al., 1997; Colombo et al., 2009).

6.1 Textural and compositional evidence for a primary crystallization of topaz in the Chivinar rhyolite

The topaz crystals in the Chivinar rhyolitic lavas show different modes of occurrence. Two of these suggest igneous textural relationships: (a) in correspondence of concentration of voids, topaz forms anhedral/subhedral grains in association with quartz (Fig. **4C-G**); (b) scattered in the matrix, topaz forms glomeroporphyritic elongate grains, again in association with quartz but without a noticeable concentration of voids. A third mode of occurrence (c) is within voids, where it shows idiomorphic terminations (Fig. **4F**) indicating crystallization in fluid-filled cavities. Topaz is never associated to secondary minerals; indeed, the Chivinar rhyolites lack any evidence of replacement of primary minerals by secondary phases out of the alteration zone (i.e. **no albite, sericite or topaz replacing plagioclase and alkali feldspar). White mica is frequently encountered in sample TG-9, but it is never found in replacement of feldspars; rather, it is interstitial in the groundmass, suggesting crystallization from the residual melt.** Moreover, the **miaroles in all the samples** are never lined or filled by secondary phases. Thus, all topaz occurrences in the Chivinar rhyolite belong to the final phases of magmatic crystallization of the rhyolitic magma.

From the point of view of the chemical composition, the presence of magmatic topaz requires a fluorine-rich and peraluminous melt. Generally, in the final stages of differentiation, rhyolitic magmas may become volatile-rich, particularly in halogens. While chlorine tends to be characteristic of peralkaline rhyolites, fluorine (and a high F/Cl) is characteristic of peraluminous rhyolites (Scaillet and MacDonald, 2004; and references therein). Fluorine tends to remain in the silicate melt until late in the magma differentiation process, having a low $D_{fluid/melt}$ (0.15-0.04 is reported in peraluminous melts, see Baker and Alletti, 2012) and is not lost into the volatile phase until very low pressures (Aiuppa et al., 2009). Thus, the F content of the final Chivinar rhyolite melt was presumably very high, also in the presence of an exsolved aqueous phase. At this stage, the peraluminous composition of the Chivinar rhyolite and the subtraction of most Ca from melt by the

279 former crystallization of plagioclase phenocrysts, favoured the crystallization of topaz in respect to
280 fluorite. Therefore, the chemistry of the Chivinar rhyolite is in agreement with the interpretation of
281 topaz as a primary, late magmatic phase.
282 Since topaz occurs in the groundmass, when it crystallized from the residual melt an aqueous fluid
283 phase was already exsolved. This is demonstrated by the presence of fluid inclusions in crystals,
284 also. The F vapour/melt partition coefficient depends on F abundance: concentrations as high as
285 ≥7–8 wt % F in melt will result in F preferentially partitioning into the fluid phase (Webster, 1990;
286 Carroll and Webster, 1994; Dolejš **and Baker,** 2007). Such high concentrations are not common in
287 nature, but could have been achieved in the very residual melt of the Chivinar rhyolite, allowing F
288 escape into the vapour phase. This explains how crystallization of topaz could continue into the
289 fluid-filled bubbles (Fig. **4F**).
290
291 *6.2 Crystallization history of the Chivinar topaz rhyolites*
292
293 The composition of the Chivinar topaz rhyolite rocks, with very low Sr and Ba and high Rb and Nb,
294 indicates that the **melt was** highly differentiated. The low phenocryst content of the Chivinar
295 rhyolitic lavas suggests a low liquidus temperature, due to the presumably high F content of the
296 silicic melt. The presence of two feldspars in equilibrium indicates subsolvus crystallization, in
297 agreement with high P-fluid. The magmatic garnet with >20 wt% MnO indicates a relatively low
298 crystallization pressure, <300 MPa, according to experimental and geological reconstructions in
299 peraluminous plutons (Miller and Stoddard, 1981 and reference therein). Therefore, the storage
300 pressure of the rhyolitic magma can be assessed at 300-400 MPa.
301 The crystallization temperature in the magma chamber, estimated from the phenocrysts - oligoclase
302 and sanidine – composition, is 720-730°C for 4 wt% H_2O, according to the geothermometer of
303 Putirka (2008) for a pressure of 300-400 MPa. As a comparison, 775+40°C to 800°C were
304 calculated for Taylor Creek rhyolite, based on two feldspar equilibrium and the Fe-oxides

305 geothermometer (Duffield and Brey, 1990). The same authors estimated 700°C to 800°C for
306 crystals in miarolitic cavities of Taylor Creek lava.
307 Quartz, sanidine and plagioclase form the groundmass crystallizing assemblage, whose nucleation
308 was in response to magma ascent**, decompression and fluid exsolution. The size, shape and**
309 **mutual relationships of the groundmass crystals, lacking the skeletal microlites indicative of**
310 **high undercooling, suggests a moderate nucleation rate, as well as moderate growth rate in**
311 **response to a rather slow cooling of the interior of the domes.** Exsolution of an aqueous fluid,
312 evidence of which remains in the abundant primary fluid inclusions in the late groundmass crystals
313 (particularly in topaz) and in the trails of secondary fluid inclusions in the phenocrysts (Fig. **4A),**
314 began early during magma ascent, but was important at the late stage of groundmass crystallization.
315 The absence of glass **and of devitrification textures** is in agreement with the low viscosity of the
316 final F-rich melt, allowing element diffusion and **complete** groundmass crystallization during the
317 final stages of cooling of the lava domes**. The isotropic texture of the rocks indicates that**
318 **crystallization took place without flowing of magma, that is after the dome emplacement.**
319 During the slow cooling **above the solidus,** crystallization of the groundmass crystals (quartz,
320 sanidine, sodic plagioclase) forced the melt composition to a very residual chemistry. The F-rich
321 and low-viscosity interstitial melt could migrate through the microlite framework (Fig. **8)**, in a
322 similar way to the gas filter-pressing process forming segregation vesicles in basaltic dykes
323 (Sanders, 1986). This mechanism permitted the formation of the quartz+topaz+vapour bubbles
324 concentrations, similar to the miaroles that form in felsic fine-grained intrusions crystallizing at
325 shallow crustal levels (Fig. **8)**. This was because the composition of the local residual magma
326 attained high fluorine content, resulting in moving the eutectic composition and enlarging the quartz
327 field. The residual melt at this point was probably of topazite, rather than ongonite, composition
328 (i.e.; Kortemeier and Burt, 1988), and the fluorine content was high enough to allow F partitioning
329 into the vapour phase and crystallization of vapour-phase topaz (Fig. **8)**.

330 The fact that the miaroles have irregular shapes, controlled by the crystals already present in the
331 groundmass, is in agreement with their formation during a late stage release of volatiles (Vernon,
332 2004; Agangi et al., 2010). Besides topaz, quartz and sporadic other minerals concluded their
333 crystallization in the fluid-filled vesicles by precipitation from the vapour phase (Candela and
334 Blevin, 1995) (Fig. **8**).
335 The rounded shape shown by quartz crystals in the groundmass may be due to the high volatile
336 content of the final interstitial melt, inhibiting crystallization. Alternatively**, taking into account**
337 **that quartz shows resorption while feldspars do not, and that the field of stability of quartz**
338 **was expanded at the expenses of feldspars by the presence of fluorine, we propose** that the
339 crystallization of topaz, decreasing **fluorine** in melt, may have resulted in quartz instability causing
340 the rounded corners**. Resorption of early quartz crystals in silicic systems may be caused by**
341 **adiabatic decompression, also, as proposed in several recent studies (e.g. Agangi et al., 2011),**
342 **but this mechanism is not suitable to explain the texture of the Chivinar rhyolites. In the**
343 **Chivinar domes, rounding affects groundmass quartz microlites in the inner dome portion,**
344 **therefore it occurred after dome emplacement; decompression of the partially molten dome**
345 **interior after dome emplacement, possibly provoked by carapace brecciation episodes, would**
346 **result in rapid microlite nucleation and growth in the residual melt, originating a texture**
347 **completely different from that observed.**
348 Cooling of the dome interior continued slowly below the solidus**. The Na-rich lamellae in alkali**
349 **feldspar crystals could represent exsolution lamellae due to feldspar unmixing, indicating that**
350 **cooling below the solidus was sufficiently slow to allow cryptoperthite development (Fig. 4G).**
351 **On the other hand, it cannot be excluded that the Na-rich lamellae indicate incipient**
352 **albitization of sanidine in the presence of a Na-bearing fluid. In this hypothesis, albitization**
353 **would represent a late, autometasomatic process in the interior of the dome. The**
354 **discrimination between the two processes is complicated by the fact that albitization develops**
355 **along the same planes of perthitic textures (Norberg et al., 2011). However, even if any**

albitization may have occurred, it must have been an incipient process without noticeable consequences on the rock composition.

6.3 Rare metals minerals

Accessory minerals in the Chivinar rhyolites account for their high content in Nb and Ta, and this is in agreement with the chemistry of the lavas. For instance, Nb-bearing rutile is one of the main accessories found in the heavy mineral fraction, and the partition coefficients DNb and DTa between rutile and melt for peraluminous magmas with ASI=1.22, the same of the Chivinar rhyolite, are reported to be close to 4900 and 1900, respectively (Linnen and Keppler, 1997). The accessories are sometimes found inside phenocrysts (Fig. **4B**) but they are often interstitial in the groundmass or even in correspondence of the vesicles. This indicates that they crystallized also from the final residual melt+vapour phase. This behaviour, already reported in volatile-rich silicic magmas (Agangi et al., 2010), supports a role of F-rich fluids in transporting immobile elements such as Nb and Ta.

The data collected so far indicate the existence, in Late Miocene, of a F-H_2O-rich and rare metal-rich magma chamber feeding the silicic Chivinar volcanic phase. This suggests that rare metals mineralizations formed in the Chivinar region **(René and Škoda, 2011).** The extent of the mineralization depends, besides the extent of the silicic magma system after the rhyolitic lava effusion, on the timing and extent of F partitioning in the fluid phase and of Nb and Ta entering accessories. The secondary mineralogy present in the Chivinar rocks, dominated by Nb-Ta-Mn oxides and silicates and devoid of chalcophile elements, and the fact that alteration affects only the rhyolitic rocks and not the younger andesite sequence, suggests a genetic link of the alteration mineralogy with the topaz rhyolite magmatic system, rather than with an andesitic one.

6.4 Geodynamic setting

In addition to the Central Andes, rhyolitic lavas with magmatic topaz have been previously found in the western United States and Mexico, in the Basin and Range Province (Burt et al., 1982; Christiansen et al., 1983, **1986,** 2007), and in the Nanling Range, in southern China (Xie et al., 2013). A common feature of these provinces is the presence of lithospheric extension in an intraplate setting, with crust-mantle interaction having an important role in the generation of the magmas. Magmatism in these provinces consisted of the intrusion of hot mafic magmas at the base and within the crust, providing a heat source for partial melting. Very similar tectono-magmatic conditions are found also for the topaz rhyolites of Chivinar, in the Central Andes. Even though Chivinar lies at the edge of the N-S trending volcanic arc of the Central Andes, its main structures are the WNW-ESE transtensive faults associated with the transverse COT structure. This suggests that, from a structural point of view, rhyolitic volcanism of Chivinar may be mostly related to the back-arc transtensive conditions of COT (Acocella et al., 2011), rather than to the arc structures. In fact, even though the overall tectonic setting of the Central Andes is contractional, transtensive or extensional conditions are found along the NW-SE trending fault zones in the back-arc (e.g. Riller et al., 2001). Among these is the transtensive COT, possibly carrying most of the extension in the Central Andes (Acocella et al., 2011). In this context, the **compositional features of the Chivinar topaz rhyolites, in particular the high Nb-Ta and low Y/Nb (Fig. 6),** could indicate partial melting of a continental crust previously intruded by mafic igneous bodies in an extensional regime, similarly to the North America topaz rhyolites (Christiansen et al., 2007). Therefore, despite the overall contractional or strike-slip setting of the arc, it is interesting to underline a connection between the **transtensive/extensional features of the COT** and intraplate extensional settings elsewhere. These similarities highlight preferred conditions for the formation of magmatic topaz.

7. Conclusions

The late magmatic origin of topaz in the Chivinar rhyolite lavas is supported by its igneous textural relationships with magmatic crystals and is in accordance with the peraluminous composition of the rhyolites. In addition, the topaz lacks any evidence of relationships with post-emplacement hydrothermal alteration. Textural evidence indicates that the phenocryst-poor lava of the domes interior underwent very slow cooling, and final crystallization took place in a large temperature interval. During the crystallization of the quartz-feldspathic groundmass, we propose that the F-rich, low-viscosity residual melt migrated in the crystal network and was concentrated, forming miaroles in which an assemblage topaz+quartz+vapour bubbles formed. In this final stage of groundmass crystallization, the F content in melt was so high that F could escape into the vapour phase, allowing also the final crystallization of topaz in the fluid-filled vesicles.

Given the magmatic origin of topaz, the topaz-bearing mineral assemblage in the Chivinar rhyolites suggests the existence of F-rich and rare metals-rich Late Miocene magma chambers. In addition, the alteration dominated by Nb-Ta-Mn oxides and silicates, affecting localized areas of the rhyolitic domes and pre-dating the following andesitic phase of the Chivinar volcano, suggests a genetic link with the topaz rhyolite magmatic system. This raises the possibility of the existence of veins or replacement deposits of rare metals, as well as of rare metals pegmatite bodies, in the Chivinar area. The extensional regime due to the presence of the transtensive COT structure suggests a correspondence with topaz rhyolites in North America and China, sharing similar geochemical features unrelated to subduction, and, thus highlights preferred conditions for the formation of magmatic topaz in overall intraplate settings.

Acknowledgements

The authors thank two anonymous reviewers for their comments and suggestions. This work has been carried out in the framework of the scientific convention between Pisa (Italy) and Salta (Argentina) Universities. The research was supported by the FONCYT-AGENCIA, (PICT Nº 0745 project), Salta University Research Council (CIUNSA-Project Nº 1861) and University of Pisa funds.

References

Acocella, V., Gioncada, A., Omarini, R., Riller, U., Mazzuoli, R., Vezzoli, L., 2011. Tectonomagmatic characteristics of the back-arc portion of the Calama-Olacapato-El Toro Fault Zone, Central Andes. Tectonics 30 TC3005 doi:10.1029/2010TC002854.

Agangi, A., Kamenetsky, V., McPhie, J., 2010. The role of fluorine in the concentration and transport of lithophile trace elements in felsic magmas: Insights from the Gawler Range Volcanics, South Australia. Chemical Geology 273, 314–325.

Agangi, A., McPhie, J., Kamenetsky, V.S., 2011. Magma chamber dynamics in a silicic LIP revealed by quartz: the Mesoproterozoic Gawler Range Volcanics. Lithos 126, 68-83.

Aiuppa, A., Baker, D.R., Webster, J.D., 2009. Halogens in volcanic systems. Chemical Geology 263, 1-18.

Baker, D.R., Alletti, M., 2012. Fluid saturation and volatile partitioning between melts and hydrous fluids in crustal magmatic systems: The contribution of experimental measurements and solubility models. Earth-Science Reviews 114, 298-324. DOI :10.1016/j.earscirev.2012.06.005.

Blasco, G., Zappettini, E.O., Hongn, F., 1996. Hoja geológica 2566−1, San Antonio de los Cobres, Programa Nac. de Carteas Geol. de la Repub. Argentina, Dirección. Nacional del Servicio Geológico, Buenos Aires, Argentina.

Breiter, K., 2012. Nearly contemporaneous evolution of the A- and S-type fractionated granites in the Krušné hory/Erzgebirge Mts., Central Europe. Lithos 151, 105-151.

459 Burt, D.M., Sheridan, M.F., Bikun, J.V., Christiansen, E.H. 1982. Topaz rhyolites: distribution,
460 origin, and significance for exploration. Economic Geology 77, 1818-1836.
461 Candela, P.A., Blevin, P.L., 1995. Do some miarolitic granites preserve evidence of magmatic
462 volatile phase permeability?. Economic Geology 90, 2310-2316.
463 Carroll, M.R., Webster, J. D., 1994. Solubilities of sulfur, noble gases, nitrogen, chlorine, and
464 fluorine in magmas Reviews in Mineralogy and Geochemistry 30, 231-279.
465 Christiansen, E.H., Burt, D.M., Sheridan, M.F., Wilson, R.T., 1983. The petrogenesis of topaz
466 rhyolites from wester united states. Contributions to Mineralogy and Petrology 83, 16-30.
467 Christiansen, E.H., Burt, D.M., Sheridan, M.F., 1986. The geology of topaz rhyolites from the
468 western United States. Geological Society of America Special Paper, 205, 82 pp.
469 Christiansen, E.H., Haapala, I., Hart, G.L. 2007. Are Cenozoic topaz rhyolites the erupted
470 equivalents of Proterozoic rapakivi granites? Examples from the western United States and
471 Finland. Lithos 97, 219-246.
472 Colombo, F., Lira, R., Pannunzio Miner, E.V., 2009. Mineralogical characterization of topaz from
473 miarolitic pegmatites and W-bearing greisen in the A-type El Portezuelo Granite, Papachacra
474 (Catamarca Province). Revista Asociación Geológica Argentina 64 (2), 194-200.
475 Dolejš, D., Baker, D.R., 2007. Liquidus equilibria in the system K_2O–Na_2O–Al_2O_3–SiO_2–F_2O1–
476 H2O to 100 MPa: II. Differentiation paths of fluorosilicic magmas in hydrous systems. Journal
477 of Petrology 48 (4), 807-828.
478 Eadington, P. J., Nashar, B., 1978. Evidence for the Magmatic Origin of Quartz-Topaz Rocks From
479 the New England Batholith, Australia. Contribution Mineralogy and Petrology 67, 433-438.
480 Duffield, W.A., Brey, E.A., 1990. Temperature, size, and depth of the magma reservoir for the
481 Taylor Creek Rhyolite, New Mexico. American Mineralogist 75, 1059-1070.
482 Huspeni, J.R., Kesler, S.E., Ruiz, J., Tuta, Z., Sutter, J.F., Jones, L.M., 1984. Petrology and
483 geochemistry of rhyolites associated with tin mineralization in northern Mexico. Economic
484 Geology 79, 87-105.

485 Irvine, T.N., Baragar, W.R.A., 1971. A guide to chemical classification of the common rocks.
486 Canadian Journal of Earth Science 8, 523-548.
487 Johannes, W., Holtz, F., 1996. Petrogenesis and Experimental Petrology of Granitic Rocks,
488 Springer-Verlag, Berlin, 335 pp.
489 Jordan, T.E., Alonso, R.N., 1987. Cenozoic stratigraphy and basin tectonics of the Andes
490 Mountains 20º-28º South Latitude. The American Association of Petroleoum Geologists
491 Bulletin 71, 49-64.
492 Keppler, H., 1993. Influence of fluorine on the enrichment of high field strength trace elements in
493 granitic rocks. Contribution to Mineralogy and Petrology 114, 479-488.
494 **Kleeman, J. D., 1985. Origin of disseminated wolframite-bearing quartz-topaz rock at**
495 **Torrington, New South Wales, Australia. High-Heat Production (HHP) Granites,**
496 **Hydrothermal Circulation and Ore Genesis. London, Institution of Mining and**
497 **Metallurgy, 197-201.**
498 Kortemeier, W.T., Burt, D.M., 1988. Ongonite and topazite dikes in the Flying W ranch area, Tonto
499 basin, Arizona. American Mineralogist 73, 507-523.
500 Koukharsky, M., Munizaga, F., 1990. Los volcanes Guanaquero, Chivinar, Tul Tul, Del Medio y
501 Pocitos, provincia de Salta, Argentina. Litología y edades K/Ar. XI Congreso Geologico
502 Argentino, San Juan, Actas 1, 64-67.
503 Koukharsky, M., Pereyra, F., Etcheverria, M, Lanes, S., 1991. La riolita con topacio del cerro
504 Chivinar, Departamento Los Andes, Provincia de Salta. Revista Asociacion Geologica
505 Argentina 46, 349-351.
506 Le Bas, M.J., Le Maitre, R.W., Streckeisen, A., Zanettin, B., IUGS Subcommission on the
507 Systematics of Igneous Rocks, 1986. A Chemical Classification of Volcanic Rocks Based on
508 the Total Alkali-Silica Diagram. Journal of Petrology 27, 745-750.

509 Linnen, R.L., Keppler, H., 1997. Columbite solubility in granitic melts: consequences for the
510 enrichment and fractionation of Nb and Ta in the Earth's crust. Contributions to Mineralogy and
511 Petrology 128, 213-227.
512 Lukkari, S., 2002. Petrography And Geochemistry Of The Topaz-Bearing Granite Stocks In
513 Artjärvi And Sääskjärvi, Western Margin Of The Wiborg Rapakivi Granite Batholith. Bulletin
514 Of The Geological Society Of Finland 74 (1–2), 115–132.
515 Manning, D.A.C., Exley, C.S., 1984. The origins of late-stage rocks in the St Austell granite—a re-
516 interpretation. Journal of the Geological Society of London 141, 581-591.
517 Matteini, M., Mazzuoli, R., Omarini, R., Cas, R., Maas, R., 2002. The geochemical variations of the
518 upper cenozoic volcanism along the Calama–Olacapato–El Toro transversal fault system in
519 central Andes (~24°S): petrogenetic and geodynamic implications. Tectonophysics 345, 211-
520 227.
521 Miller, C.F., Stoddard, E.F., 1981. The role of manganese in the paragenesis of magmatic garnet: an
522 example from the old Woman-Piute range, California. Journal of Geology 89: 233-246.
523 **Norberg, N., Neusser, G., Wirth, R., Harlow, D., 2011. Microstructural evolution during**
524 **experimental albitization of K-rich alkali feldspar. Contribution to Mineralogy and**
525 **Petrology 162, 531-546.**
526 Morimoto, N., 1988. Nomenclature of pyroxenes. Mineralogical Magazine 52, 535-55.
527 Orlandi, P., Gioncada, A., Vezzoli, L., Omarini, R., Mazzuoli, R., Lopez-Azarevich, V., Sureda, R.,
528 Azarevich, M., Bianchi, D., Acocella, V., Rusch, J., Guillou, H., Nonnotte, P., 2011. The topaz-
529 bearing rhyolite lavas from Chivinar volcanic complex (24°17’38’’S - 67°25’28’’W, Central
530 Andes, NW Argentina). 1er Simposio sobre petrología ígnea y metalogénesis asociada. San
531 Miguel de Tucumán, November 16-18, 2011.
532 Putirka, K., 2008. Thermometers and Barometers for Volcanic Systems. In: Putirka, K., Tepley, F.
533 (Eds.), Minerals, Inclusions and Volcanic Processes, Reviews in Mineralogy and Geochemistry,
534 Mineralogical Soc. Am., 69, 61-120.

René, M., Škoda, R., 2011. Nb-Ta-Ti oxides fractionation in rare-metal granites: Krásno-Horní Slavkov ore district, Czech Republic. Mineralogy and Petrology 103, 37–48. DOI 10.1007/s00710-011-0152-z.

Riller, U., Petrinovic, I., Ramelow, J., Strecker, M., Oncken, O., 2001. Late Cenozoic tectonism, collapse calderas and plateau formation in the Central Andes. Earth Planetary Science Letters, 188, 299-311.

Rodríguez-Ríos, R., Aguillón-Robles, A., Leroy, J. L., 2007. Evolución petrológica y geoquímica de un complejo de domos topacíferos en el Campo Volcánico de San Luis Potosí (México). Revista Mexicana de Ciencias Geológicas 24 (3), 328-343.

Salfity, J.A., 1985. Lineamentos transversales al rumbo andino en el noroeste argentino. In: Actas IV Congreso Geológico Chileno, Antofagasta, Chile, 2, 119–137.

Sanders, I.S., 1986. Gas filter-pressing origin for segregation vesicles in dykes. Geological Magazine 123, 67-72.

Scaillet, B., Macdonald, R., 2004. Fluorite stability in silicic magmas. Contributions to Mineralogy and Petrology 147, 319–329.

Sinclair, W.D., 1986. Early Tertiary topaz rhyolites and associated mineral deposits in the northern Canadian Cordillera; products of anorogenic magmatism. Program with abstracts — Geological Association of Canada. Mineralogical Association of Canada Annual Meeting, 11, 127–128.

Sun, S., McDonough, W.R., 1989. Chemical and isotopic systematics of oceanic basalts: implications for mantle composition and processes. In Saunders, A. D. & Norry, M. J. (eds), 1989, Magmatism in the Ocean Basins, Geological Society Special Publication 42, 313-345.

Taylor, R.P., 1992. The petrological and geochemical characteristics of the Pleasant Ridge zinnwaldite-topaz granite, southern New Brunswick, and comparisons with other topaz-bearing felsic rocks. The Canadian Mineralogist 30, 895-921.

560 Taylor, R., 2009. Ore textures - Recognition and interpretation. Springer-Verlag, 282 pag., ISBN
561 978-3-642-01782-7.
562 Taylor, R.P., Fallick, A.E., 1997. The evolution of fluorine-rich felsic magmas: source dichotomy,
563 magmatic convergence and the origins of topaz granite. Terra Nova 9 (3), 105-108.
564 Tuttle, O.F., Bowen N.L. 1958. Origin of Granite in the Light of Experimental Studies in the
565 System $NaAlSi_3O_8$-$KAlSi_3O_8$-SiO_2-H_2O. Geological Society of America 74, 153 p.
566 Vernon, R.H., 2004. A Practical Guide to Rock Microstructure. Cambridge University Press.
567 Webster, J.D., 1990. Partitioning of F between H_2O and CO_2 fluids and topaz rhyolite melt
568 Implications for mineralizing magmatic-hydrothermal fluids in F-rich granitic systems
569 Contributions to Mineralogy and Petrology 104, 424-438.
570 **Whalen, J.B., Currie, K.L., Chappell, B.W., 1987. A-type granites; geochemical**
571 **characteristics, discrimination and petrogenesis. Contributions to Mineralogy and**
572 **Petrology 95, 407–419.**
573 Williamson, B.J., Stanley, C.J., Wilkinson, J.J., 1997. Implications from inclusions in topaz for
574 greisenisation and mineralisation in the Hensbarrow topaz granite, Cornwall, England.
575 Contributions to Mineralogy and Petrology 127, 119-128.
576 **Xie, L., Wang R., Chen, J., Zhu, J., Zhang, W., Lu, J., Zhang, R., 2013. A tin-mineralized**
577 **topaz rhyolite dike with coeval topaz granite enclaves at Qiguling in the Qitianling tin**
578 **district, southern China. Lithos 170, 52–268.**
579

Figure captions

Fig. 1. Geological framework of the Chivinar volcanic complex. (A) Location of the studied area with respect of the morpho-structural units of the Central Andes. The Western Cordillera is the active magmatic arc. Miocene to Quaternary volcanism develops in the backarc along some transverse NW-trending lineaments as the Calama-Olacapato-El Toro (COT) fault system. (B) Regional geologic map of the Puna plateau showing the location of the Chivinar volcano at the boundary between the magmatic arc and backarc. SAC: San Antonio de los Cobres. (C) Geologic map of the Chivinar volcano based on our new field mapping. Location of the samples studied is shown.

Fig. 2. Fig. 2. Field photos of volcanic features of the Cerro Chivinar volcanic complex. Location of the studied samples is also shown. (A) The northern flank of the Cerro Chivinar shows three superposed and distinct eruptive packages, from bottom: TR = topaz-bearing rhyolite lava domes; Mb = dacite megabreccia and pumice deposits; Lc = andesite lava cone. The red line is the trace of the major NW-SE striking transtensive fault (white circles indicate a sinistral kinematics). (B) The western flank of the Cerro Chivinar shows the stratigraphic and intrusive relationships between the topaz-bearing rhyolite lava domes (TR) and the Eocene-Miocene sedimentary substratum (Rp = red pelites; Gy = gypsum). Af = alluvial fan. Red lines are the traces of the major NW-SE transtensive (white circles indicate a sinistral kinematics) and NS transpressive striking faults.

Fig. 3. Composition of feldspars of the topaz rhyolites reported in the ternary An **(anorthite)**-Ab **(albite)**-Or **(orthoclase)** diagram. The composition of the primary feldspars of the rhyolitic lavas in the alteration zone is also reported.

Fig. 4. Petrographic thin section photos with crossed nicols (A, B) and backscattered electrons SEM images (C…J) of Chivinar topaz rhyolite samples. A. Fluid inclusions trails in plagioclase phenocryst (arrow shows an example). B. Sanidine phenocryst and zircon, xenotime accessories in the holocrystalline, equant, quartz-feldspathic groundmass. C. Topaz

606 concentration with voids. D. Cryptoperthitic lamellae in alkali feldspar in the topaz rhyolite,
607 testifying the final slow cooling phase of the lava dome; note the homogeneous core,
608 representative of a former crystallization step at higher temperature. E. Zircon in void, in
609 epitaxis with xenotime. F. Topaz, with syntaxial growth. G. Textural relationships between
610 topaz and quartz (arrow indicates quartz-topaz contact). Note the frequent fluid inclusions in
611 topaz. H. **Di-octahedral mica** flakes in the groundmass of Chivinar rhyolites**, sample TG-9.** I.
612 Detail of veinlet in Chivinar rhyolite. Secondary minerals in vein are Mn-bearing amphiboles
613 and Nb-bearing oxide. J. Detail of the rhyolite hosting veinlet in I: note the disseminated Nb-Ta-
614 Ti oxides**, compared to the rhyolite lava in C.**

615 Fig. **5. A. C**omposition of the Chivinar rhyolites **(open circles)** reported in the TAS diagram (total
616 alkali vs. silica, le Bas et al., 1986) and compared with the fields for topaz rhyolites from
617 Christiansen et al. (2007) (light grey) and from Rodríguez-Ríos et al. (2007) (dark grey); the
618 dashed line divides alkaline and subalkaline rocks after Irvine and Baragar (1971). The Chivinar
619 andesitic rocks are also reported **as black dots.** B. Rare Earth Element patterns of the Chivinar
620 topaz rhyolites normalized to chondrite after Sun and MacDonough (1989). **Symbols and fields**
621 **as in Figure 5A.** C. Multielement **spiderdiagrams** of the Chivinar topaz rhyolites normalized
622 to Primitive Mantle after Sun and MacDonough (1989). **Symbols and fields as in Figure 5A.**

623 **Fig. 6. Chivinar topaz rhyolites plotted in the discrimination diagram for intraplate setting**
624 **after Whalen et al. (1987). Open circles are Chivinar topaz rhyolites from this work (the**
625 **two samples nearly coincide); light grey field is topaz rhyolites from Christiansen et al.**
626 **(2007), white field is from Rodríguez-Ríos et al. (2007), dark grey field is from Xie et al.**
627 **(2013).**

628 **Fig. 7**. The "granite" system (Qz–Ab–Or) with the composition of Chivinar topaz rhyolite rocks
629 **(open circles).** The solid line indicates the quartz–feldspar cotectic and the minimum melt
630 composition at 1 kbar, H_2O-saturated conditions (Tuttle and Bowen, 1958). The arrow shows
631 the eutectic variation for F added to the haplogranite composition (Johannes and Holtz, 1996;

and references therein). Grey field is topaz rhyolites from Christiansen et al. (2007) and white field is topaz granites from Taylor and Fallick (1997).

Fig. **8.** Conceptual model of formation of the topaz+quartz+voids association in the Chivinar rhyolite.

Table captions

Table 1. Representative **EDS** analyses of primary minerals in the Chivinar rhyolitic lavas.

Table 2. Representative **EDS** analyses of secondary minerals in the Chivinar altered rhyolitic lavas.

Table 3. A. Whole rock major element composition and CIPW norm of the analyzed Chivinar rocks. ASI: Alumina Saturation Index, molecular $[Al_2O_3]/[CaO]-1.67*[P_2O_5]+[Na_2O]+[K_2O]$. B. Trace element composition of the Chivinar topaz rhyolites.

Figure_1
Click here to download high resolution image

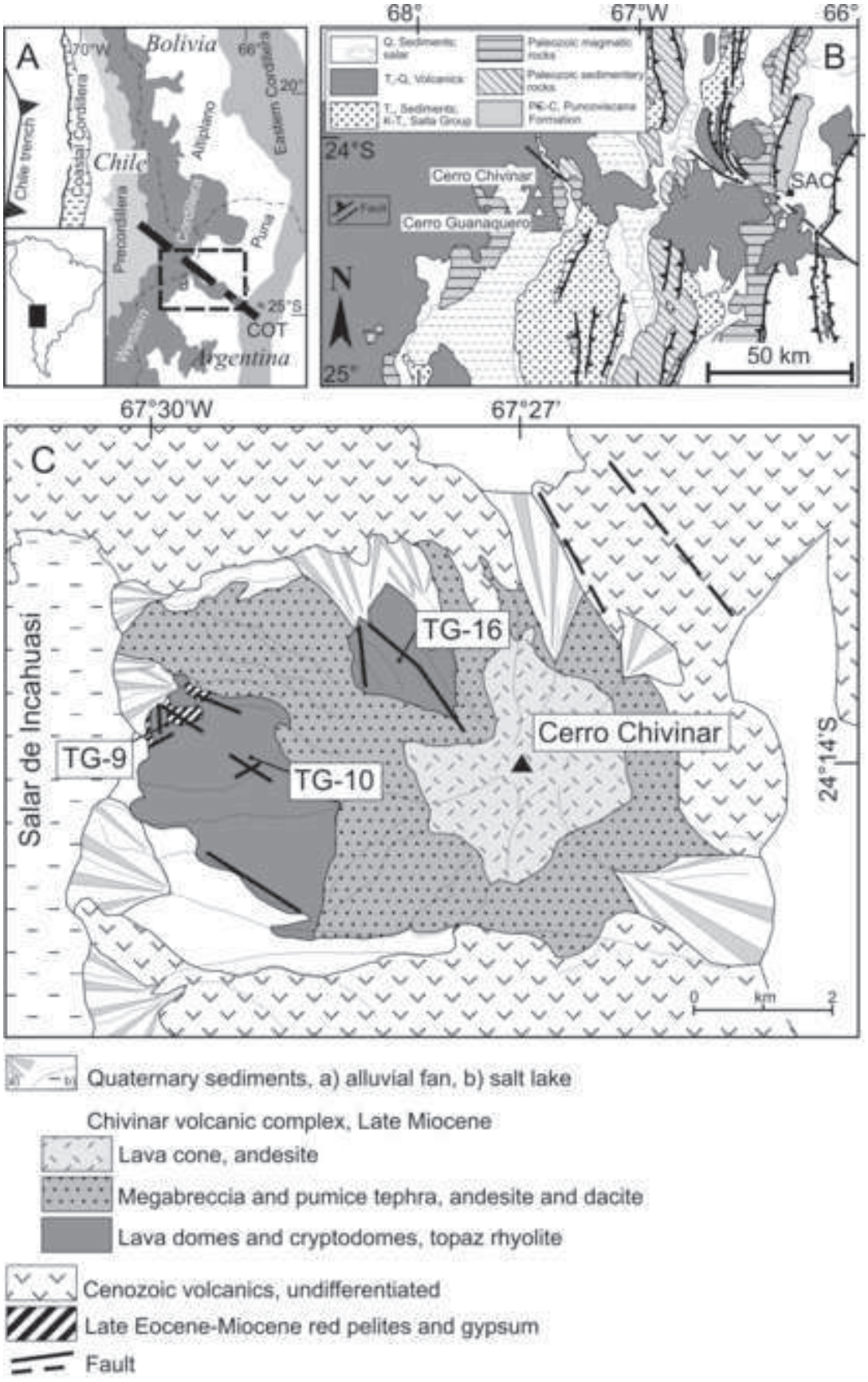

Gioncada et al Figure 1

Figure_2
Click here to download high resolution image

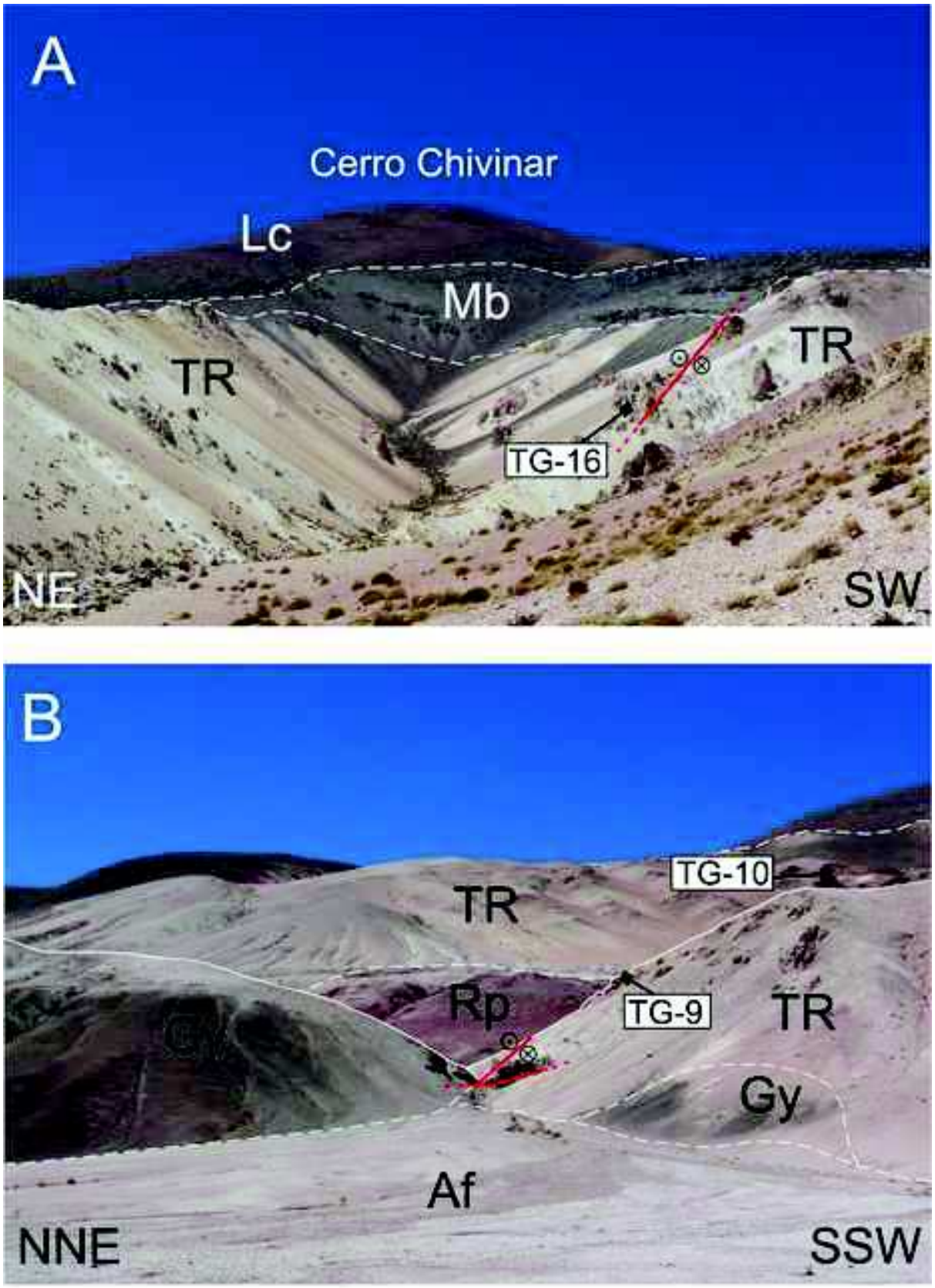

Gioncada et al. Fig.2

Figure_3

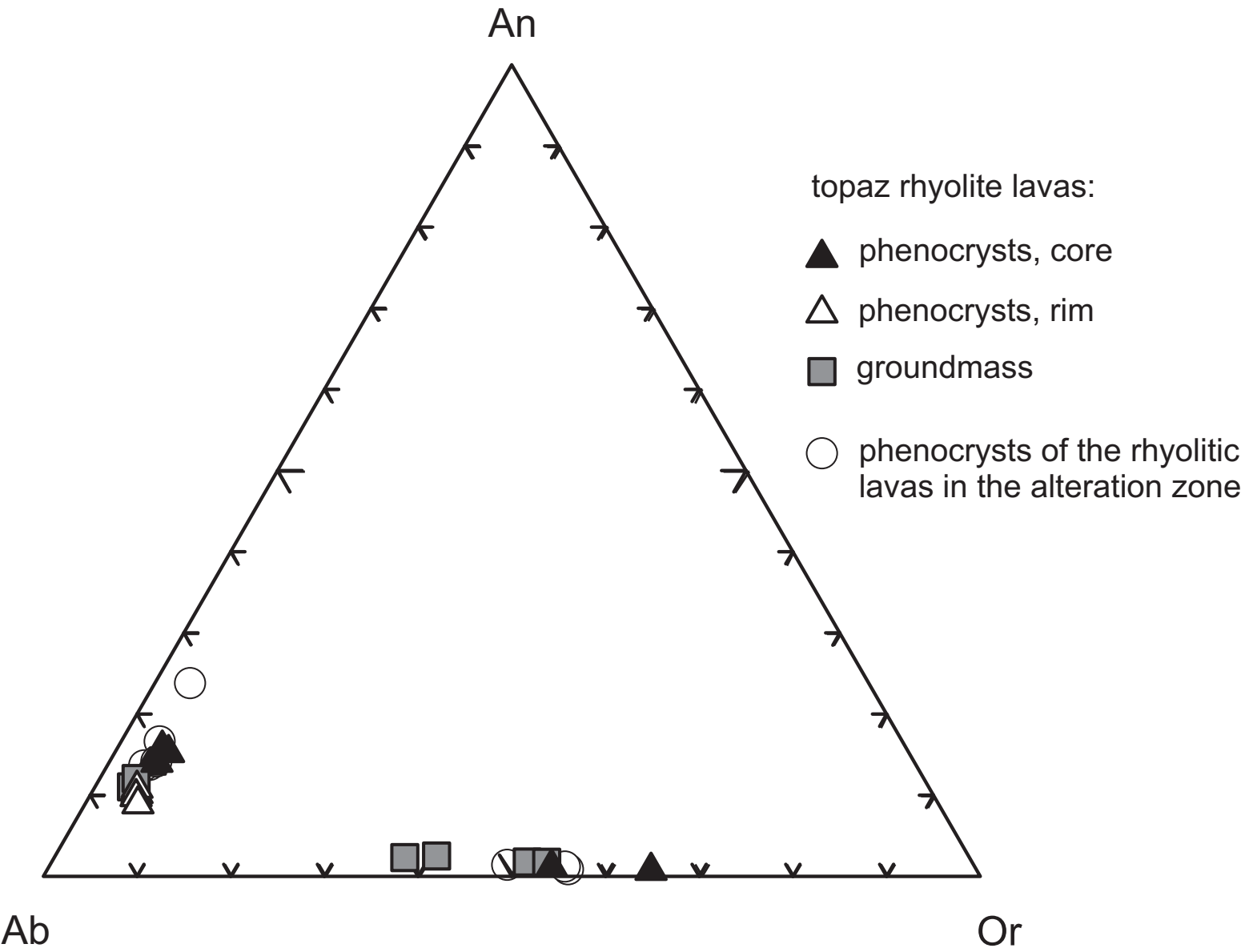

Gioncada et alii Figure 3

Figure_4
Click here to download high resolution image

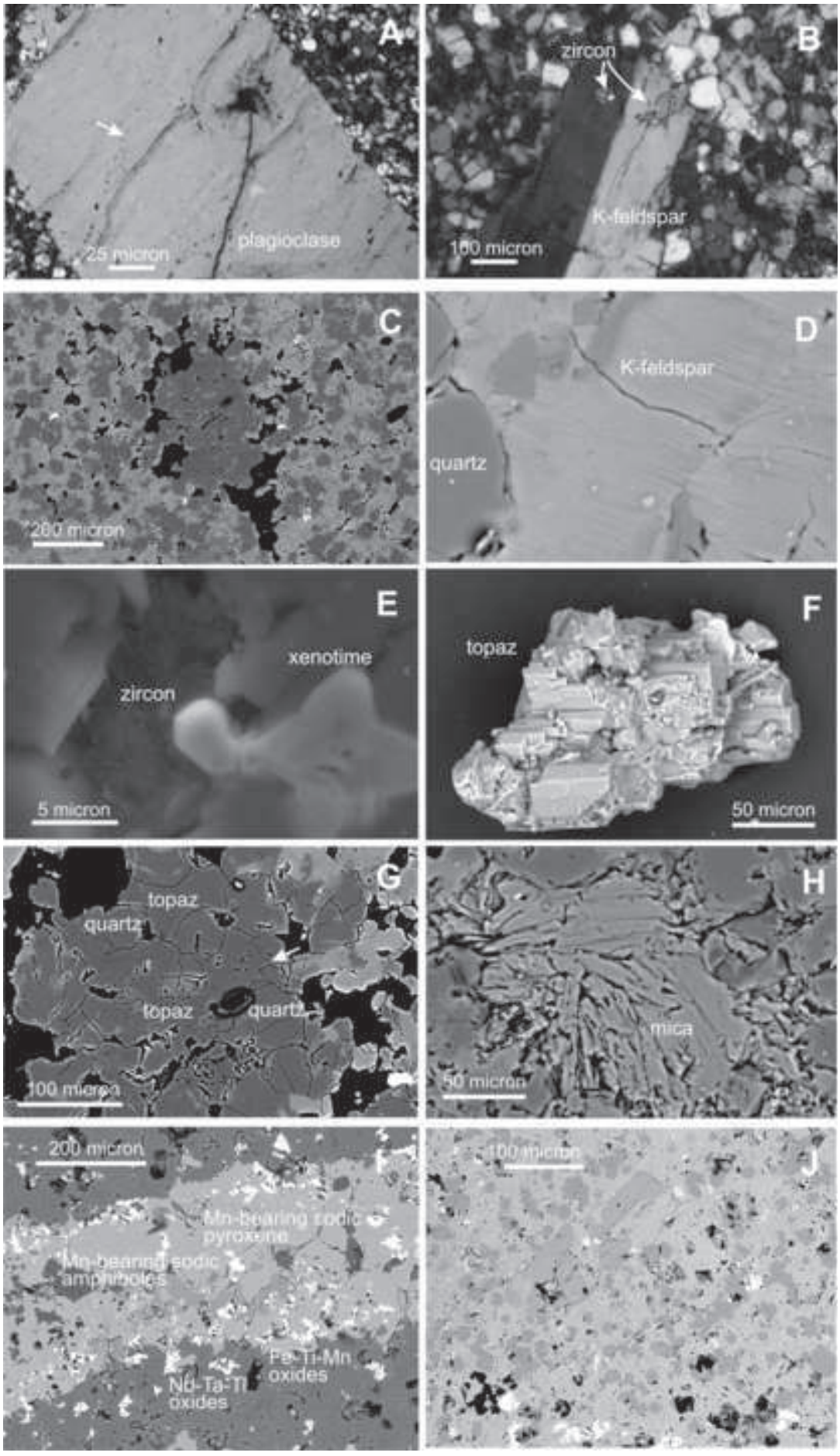

Figure_5
Click here to download high resolution image

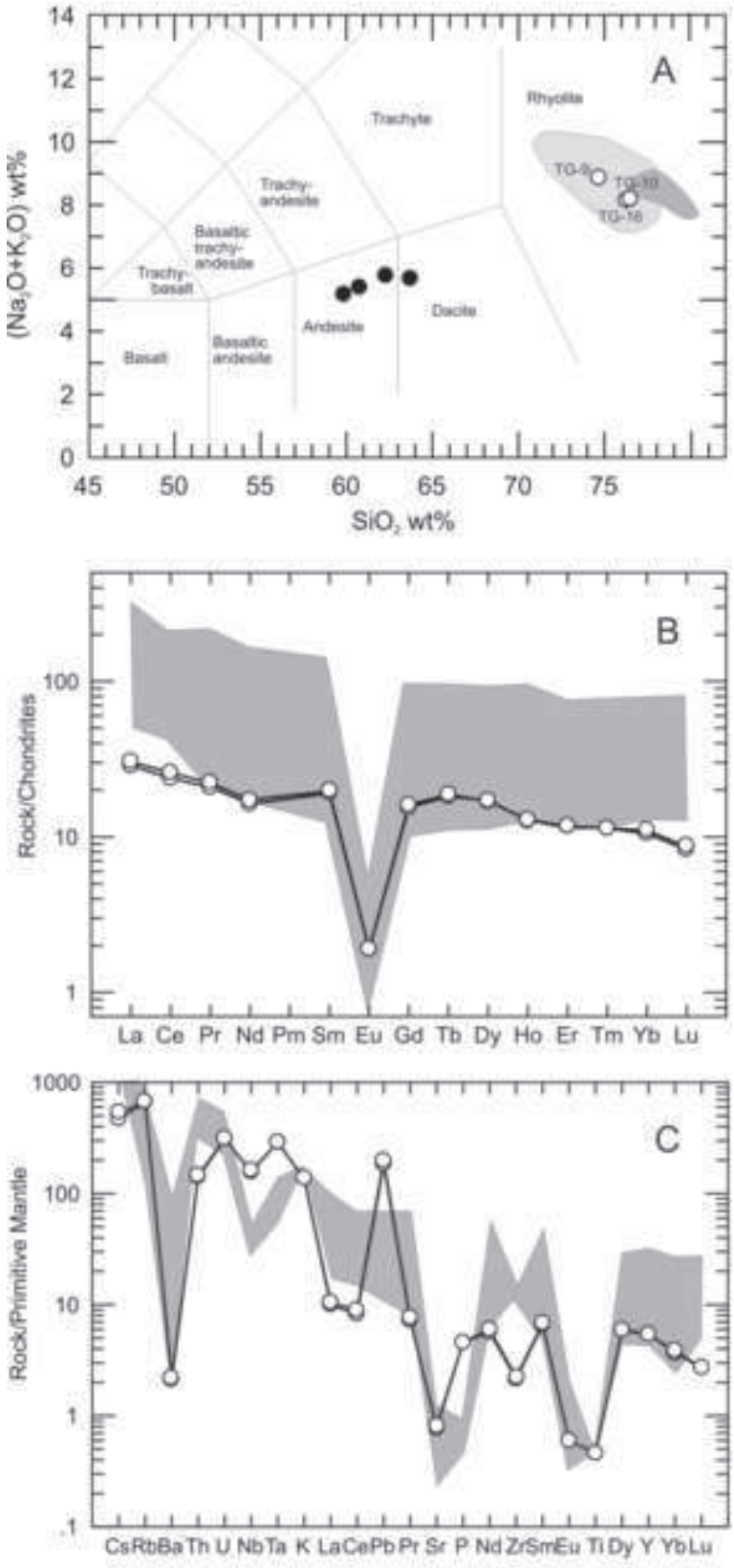

Gioncada et alii Figure 5

Figure_6
Click here to download high resolution image

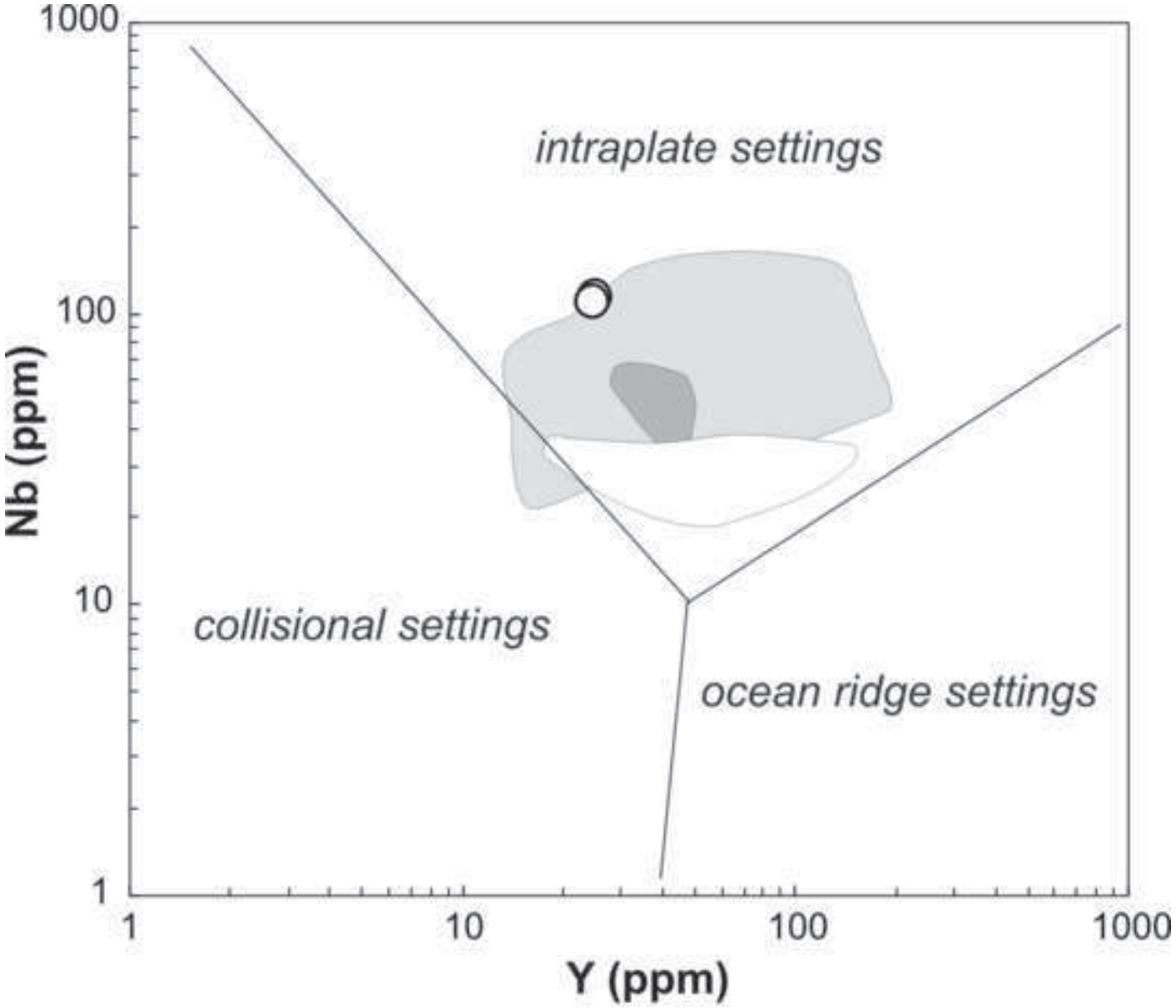

Gioncada et alii Figure 6

Figure_7
Click here to download high resolution image

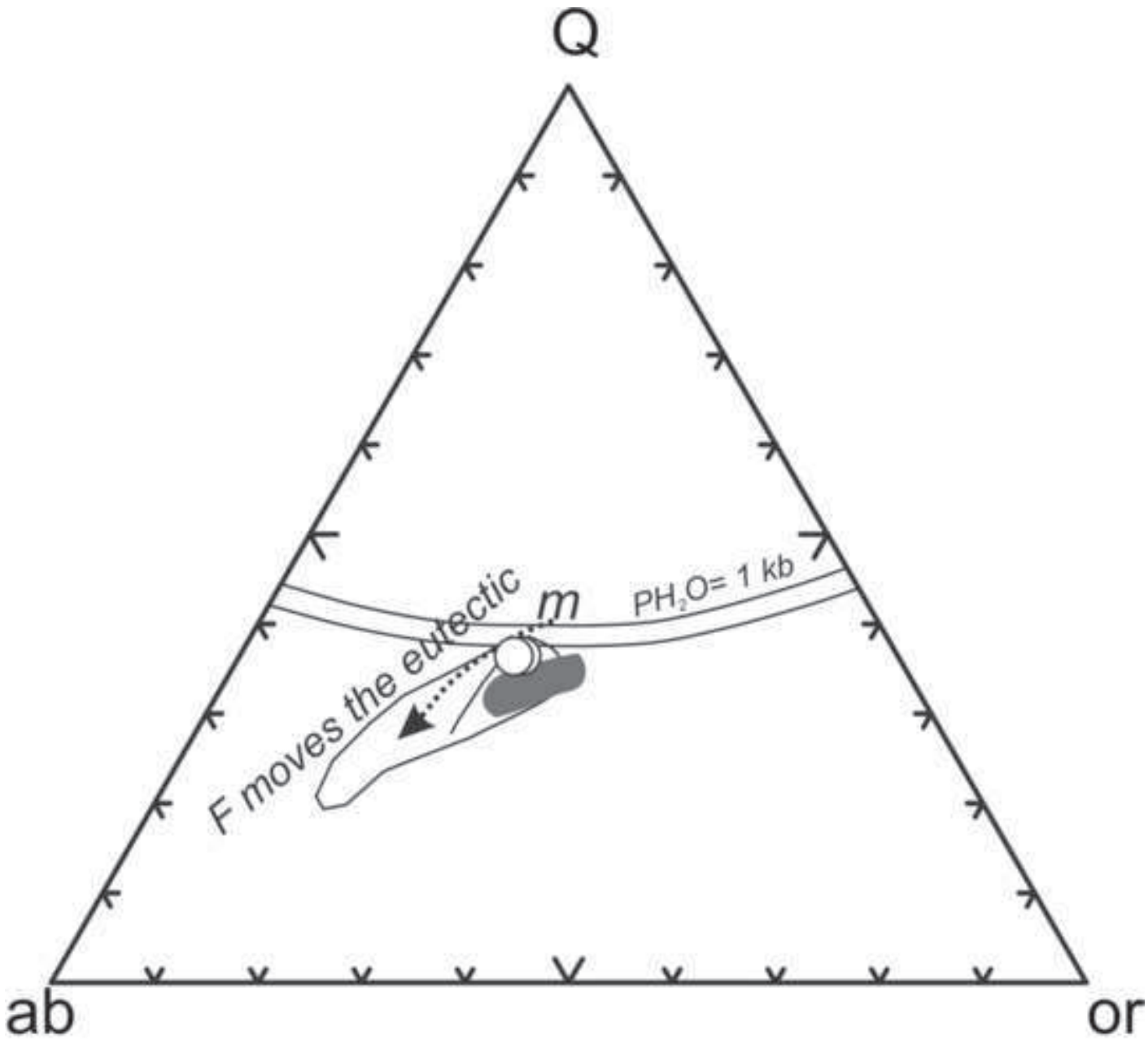

Gioncada et alii Figure 7

Figure_8
Click here to download high resolution image

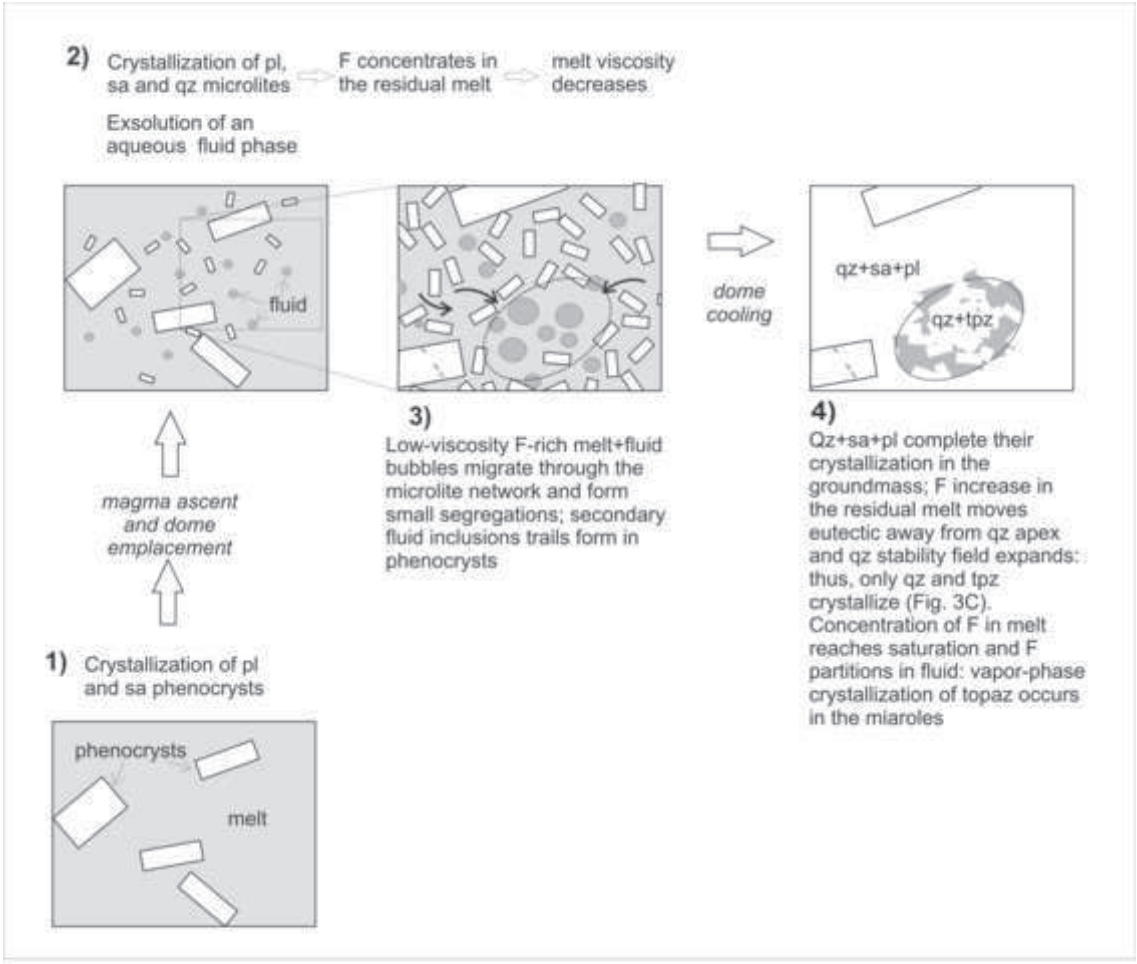

Gioncada et alii Figure 8

Table_1
Click here to download Table: Gioncada_Table_1_rev.doc

Gioncada et alii_Table 1

sample	TG-16 *pl*	TG-16 *pl*	TG-16 *pl*	TG-16 *pl*	TG-16 *pl*	TG-16 *pl*	TG-9 *pl*	TG-16 *pl*	TG-16 *pl*	TG-16 *Kf*	TG-16 *Kf*	TG-16 *Kf*	TG-9 *Kf*
wt %	core	rim	core	rim	core	rim	core	grm	grm	core	grm	grm	grm
SiO_2	64.37	65.38	64.09	65.90	63.46	65.46	63.61	65.30	64.76	65.29	65.70	65.52	65.12
Al_2O_3	22.49	21.71	22.70	21.58	23.11	22.03	23.02	21.80	22.67	19.53	19.49	19.43	19.36
FeO	bdl	0.15	bdl	0.07	0.14	bdl	bdl	bdl	0.26	bdl	bdl	0.20	0.07
CaO	2.86	1.86	3.15	1.99	3.28	2.07	3.42	2.32	2.40	0.14	0.37	0.36	0.24
Na_2O	9.48	9.90	9.06	9.59	9.15	9.59	9.03	9.89	9.26	3.94	5.50	5.23	3.62
K_2O	0.81	1.00	1.01	0.86	0.85	0.85	0.92	0.69	0.65	11.11	8.94	9.26	11.60
An	13.63	8.87	15.18	9.77	15.73	10.13	16.40	11.03	12.04	0.68	1.76	1.73	1.16
Ab	81.77	85.45	79.02	85.20	79.41	84.92	78.35	85.07	84.08	34.78	47.47	45.39	31.80
Or	4.60	5.68	5.80	5.03	4.85	4.95	5.25	3.90	3.88	64.53	50.77	52.88	67.04

sample	TG-16 *garnet*	TG-16 *garnet*		TG-16 *tri-oct. mica*		TG-9 *di-oct. mica*	TG-9 *di-oct. mica*		TG-16 *topaz*
wt %			wt %					wt %	
SiO_2	37.15	34.9	SiO_2	41.90		51.74	51.01	SiO_2	33.55
Al_2O_3	20.92	20.86	TiO_2	0.99		0.08	0.22	Al_2O_3	49.32
FeO	15.81	16.34	Al_2O_3	20.71		31.18	31.22	$F^{(1)}$	17.13
MnO	24.11	25.82	FeO	13.39		1.82	1.78		
MgO	1.54	1.36	MnO	4.06		0.12	0.11		
CaO	0.47	0.72	MgO	7.92		3.79	3.84		
			Na_2O	bdl		0.66	0.5		
$[Al^{VI}. Fe^{2+}]$	4.04	3.85	K_2O	11.04		10.61	11.32		
[Mn. Mg. Ca]	5.92	6.34							

(1) semi-quantitative; bdl: below detection limit. Pl: plagioclase; Kf: alkali feldspar; grm: groundmass.

Table_2a

Click here to download Table: Gioncada_Table_2a_rev.doc

Gioncada et alii_Table 2a

sample	18589	18589	18589	18589	18589	18589	18589	18589
	primary feldspars					secondary feldspars		
	grdm	grdm	c	r	r	vein	vein	vein
SiO2	65.84	66.09	65.49	65.33	65.58	65.72	65.66	65.79
Al2O3	19.08	19.24	19.34	19.87	19.67	19.41	19.76	19.12
FeO	1.44	bdl	0.14	0.06	0.05	0.34	0.09	0.25
CaO	bdl	bdl	bdl	bdl	0.13	0.06	0.24	bdl
Na2O	5.25	4.81	4.26	4.97	4.99	4.93	5.75	4.75
K2O	8.39	9.86	10.77	9.77	9.58	9.54	8.5	10.09
	100.0	100.0	100.0	100.0	100.0	100.0	100.0	100.0
recalculated based on 8 oxygens								
Si	2.97	2.98	2.97	2.95	2.96	2.97	2.96	2.98
Al	1.02	1.02	1.03	1.06	1.05	1.03	1.05	1.02
Fe	0.05	0.00	0.01	0.00	0.00	0.01	0.00	0.01
Ca	0.00	0.00	0.00	0.00	0.01	0.00	0.01	0.00
Na	0.46	0.42	0.37	0.44	0.44	0.43	0.50	0.42
K	0.48	0.57	0.62	0.56	0.55	0.55	0.49	0.58
An	0.00	0.00	0.00	0.00	0.63	0.29	1.16	0.00
Ab	48.75	42.58	37.55	43.60	43.91	43.86	50.11	41.71
Or	51.25	57.42	62.45	56.40	55.46	55.84	48.74	58.29

c: core; r: rim; grdm: groundmass; bdl: below detection limit.

Table_2b

Click here to download Table: Gioncada_Table_2b_rev.doc

Gioncada et alii_Table 2b

sample	18589	18589	18589	18589	18589	18589	18589	18589
	vein	vein	vein	vein	vein	vein	vein	vein
	Mn-bearing sodic amphibole	Mn-bearing sodic amphibole	Mn-bearing sodic amphibole	Mn-bearing sodic pyroxene	Mn-bearing sodic pyroxene	Mn-bearing sodic pyroxene	Mn-bearing sodic pyroxene	Mn-bearing sodic pyroxene
SiO_2 (wt%)	58.96	58.08	58.63	53.93	53.45	55.28	54.31	54.34
TiO_2	bdl	bdl	bdl	bdl	bdl	bdl	bdl	bdl
Al_2O_3	0.91	0.42	0.61	0.28	0.25	0.83	0.75	0.87
FeO	19.29	21.26	21.26	29.07	27.3	29.04	26.74	28.06
MnO	4.82	5.97	5.55	4.14	6.53	2.8	5.27	4.21
MgO	6.36	4.52	4.45	0.2	0.97	0.38	0.77	0.68
CaO	0.26	0.56	0.63	3.18	4.35	0.56	3.75	2.03
K_2O	8.45	8.46	8.16	9.2	7.15	11.11	8.42	9.81
Na_2O	0.96	0.72	0.71	bdl	bdl	bdl	bdl	bdl
Total	100.01	100	100	99.99	100	100.01	100	100.00
	Cations recalculated on the basis of 23 oxygens			Cations recalculated on the basis of 6 oxygens				
Si	8.542	8.565	8.616	2.08	2.09	2.09	2.10	2.078
Al vi	0.155	0.073	0.106	0.01	0.01	0.04	0.03	0.039
Fe3+	0.128	0.065	0.006	0.51	0.34	0.59	0.40	0.532
Fe2+	2.209	2.558	2.607	0.43	0.55	0.33	0.46	0.365
Mn	0.591	0.746	0.691	0.14	0.22	0.09	0.17	0.136
Mg	1.374	0.994	0.975	0.01	0.06	0.02	0.04	0.039
Ca	0.040	0.088	0.099	0.13	0.18	0.02	0.16	0.083
Na	2.374	2.419	2.325	0.69	0.54	0.82	0.63	0.727
K	0.177	0.135	0.133	0.00	0.00	0.00	0.00	0.00

bdl: below detection limit.

Table_2c

Click here to download Table: Gioncada_Table_2c_rev.doc

Gioncada et alii_Table 2c

sample	18589 Fe-Mn-Ti oxide	18589 Fe-Mn-Ti oxide	18589 Mn-bearing phillosilicate	18589 Mn-bearing phillosilicate	18589 Mn- apatite	18601 Nb-Ta-bearing rutile	18601 Nb-Ta-bearing rutile	18601 Nb-Ta-bearing rutile
SiO_2 (wt%)			40.83	41.92				
TiO_2	2.98	6.86	2.48	1.96		61.71	56.96	55.82
Al_2O_3	3.23	bdl	18.67	20.25				
FeO	82.39	83.54	11.08	9.62		15.53	17.08	14.57
MnO	11.02	8.18	5.68	5.36	7.21			
MgO	0.38	bdl	9.76	9.76				
CaO					59.07			
K_2O			10.36	10.34				
Na_2O			0.49	0.6				
P_2O_5					33.73			
ZnO	bdl	1.41	0.66	0.2				
Nb_2O_5						18.72	23.73	23.77
Ta_2O_5						4.05	2.23	4.74
Total	100.00	99.99	100.01	100.01	100.01	100.01	100.00	98.90

bdl: below detection limit

Table_3a
Click here to download Table: Gioncada_Table_3a_rev.doc

Gioncada et alii_Table 3 a

sample	TG 17	TG 11	TG 18	TG 14	TG9	TG16	TG10
SiO_2 (wt%)	59.85	60.74	62.14	63.78	74.68	76.43	76.49
TiO_2	0.96	0.88	0.73	0.75	0.06	0.05	0.05
Al_2O_3	16.98	16.92	16.84	16.20	14.16	14.41	14.42
$Fe_2O_{3\ tot.}$	7.06	6.80	6.08	5.55	0.39	0.23	0.20
MnO	0.13	0.12	0.10	0.10	0.01	0.02	0.02
MgO	3.03	2.81	2.37	2.48	0.30	0.05	0.08
CaO	6.50	6.11	5.69	5.19	1.42	0.54	0.50
Na_2O	2.96	3.05	3.32	2.89	4.25	4.08	4.00
K_2O	2.19	2.26	2.42	2.79	4.64	4.10	4.15
P_2O_5	0.33	0.31	0.31	0.28	0.08	0.09	0.09
LOI	0.78	1.34	1.55	2.50	1.65	0.87	0.93
ASI	0.91	0.93	0.93	0.96	0.98	1.20	1.21
q	14.1	15.15	16.21	20.13	28.9	36.0	36.4
pl	52.0	51.93	52.29	47.65	41.8	36.6	35.7
or	13.0	13.41	14.36	16.55	27.5	24.2	24.5
c	0.0	0.0	0.0	0.0	0.0	2.5	2.7
di	3.0	2.10	1.93	0.75	0.5	0.0	0.0
hy	13.9	13.51	11.76	11.23	0.8	0.3	0.3
il	1.8	1.69	1.39	1.42	0.1	0.1	0.1
mt	1.6	1.49	1.33	1.61	0.2	0.1	0.1
ap	0.8	0.72	0.72	0.65	0.2	0.2	0.2

$Fe_2O_{3\ tot.}$: all Fe recalculated as Fe_2O_3

Table_3b

Click here to download Table: Gioncada_Table_3b_rev.doc

Gioncada et alii_Table 3 b

sample	TG10	TG16
Ba (ppm)	15.3	14.7
Co	<0.5	0.6
Cr	10	<10
Cs	3.71	4.16
Cu	<5	9
Ga	34.5	33.3
Hf	2.1	2.2
Mo	<2	<2
Nb	113	111
Ni	<5	<5
Pb	13	14
Rb	419	426
Sn	2	1
Sr	17.1	16.2
Ta	11.7	11.8
Th	11.8	12.25
Tl	1.7	1.7
U	6.47	6.63
V	5	<5
W	3	3
Y	24.9	24.5
Zn	23	27
La	6.8	7.2
Ce	14.6	15.8
Pr	1.98	2.11
Nd	7.6	8.1
Sm	2.91	3.01
Eu	0.11	0.11
Gd	3.18	3.29
Tb	0.68	0.7
Dy	4.36	4.3
Ho	0.72	0.73
Er	1.93	1.93
Tm	0.29	0.29
Yb	1.78	1.87
Lu	0.21	0.22
(La/Yb)n	2.46	2.48
Eu*/Eu	0.11	0.11